Article

A Theoretical Study of Scattering of Electrons and Positrons by CO_2 Molecule

M. Masum Billah [1] , **M. Mousumi Khatun** [1] , **M. M. Haque** [1,*] , **M. Yousuf Ali** [1] , **Mahmudul H. Khandker** [1] , **A. K. F. Haque** [1,2] , **Hiroshi Watabe** [2] and **M. Alfaz Uddin** [3]

1 Atomic and Molecular Physics Laboratory, Department of Physics, University of Rajshahi, Rajshahi 6205, Bangladesh; masumphy@ru.ac.bd (M.M.B.); mstmou2018@gmail.com (M.M.K.); mdyali13@gmail.com (M.Y.A.); kmhasanphy@yahoo.com (M.H.K.); fhaque@ru.ac.bd (A.K.F.H.)
2 Division of Radiation Protection and Safety Control, Cyclotron and Radioisotope Center, Tohoku University, 6-3 Aoba, Aramaki, Aoba, Sendai 980-8578, Japan; watabe@cyric.tohoku.ac.jp
3 Department of Physics, Pabna University of Science and Technology, Pabna 6600, Bangladesh; uddinmda@yahoo.com
* Correspondence: mhpdru@gmail.com; Tel.: +880-1716-346-268

Abstract: This article presents a theoretical investigation of the differential, integrated, elastic, inelastic, total, momentum-transfer, and viscosity cross-sections, along with the total ionization cross-section, for elastically scattered electrons and positrons from a carbon dioxide (CO_2) molecule in the incident energy range of $1 \, \text{eV} \leq E_i \leq 1 \, \text{MeV}$. In addition, for the first time, we report the spin polarization of $e^{\pm}-CO_2$ scattering systems. The independent atom model (IAM) with screening correction (IAMS) using a complex optical potential was employed to solve the Dirac relativistic equation in partial-wave analysis. The comparison of our results with the available experimental data and other theoretical predictions shows a reasonable agreement in the intermediate- and high-energy regions.

Keywords: electron and positron scattering; carbon dioxide molecule; independent atom model; screening correction; spin polarization

1. Introduction

Projectile–atom/molecule scatterings are very common in many natural and man-made systems, such as gaseous plasma [1], planetary atmospheres [2], radiation chemistry [3], radiobiology [3], mass spectrometry [4], etc. Accurate data of various observables of such scattering phenomena are, therefore, of crucial importance for the enhancement of our knowledge about the science of planetary, stellar, and interstellar spaces and for the development of technologies. In particular, the electron (e^-) impact scattering from atmospheric molecules is indispensable for the study of physical and chemical models, such as the electron-transport properties of gases, photochemistry of the atmosphere, atmospheric auroral emissions, treatment of biomaterials, and plasma discharges [5].

Positron (e^+) scattering augments the understanding of e^-−atom interaction. Because of the static component, apart from their difference in sign, the large r dependences of the polarization potential and the absorption potential are the same in the two interactions. It is well known that, whereas the net interaction for e^-−atom scattering is attractive at all energies, the net interaction for e^+−atom scattering is attractive only at low energies (up to the Ps formation threshold), and after that, it becomes repulsive. So, the study of e^- and e^+ collisions with the same target can unravel more information about projectile–target collision dynamics. Our recent calculations [6–12] of various scattering observables for $e^{\pm}$−atom systems have produced reasonable agreement with the available data. We thus now extend our calculations for $e^{\pm}$ scattering from molecular targets in order to characterize these scattering systems.

Carbon compounds are the most significant constituents of the atmosphere [13]. They are fundamental, especially for the organic chemistry taking place in the atmosphere.

Carbon dioxide (CO$_2$) is a linear, triatomic, non-polar, heteronuclear molecule. This iso-electronic molecule is the most abundant constituent of the atmospheres of Venus and Mars [14]. For the understanding of the aurora and day-glow phenomena, a comprehensive knowledge of the cross-sections of the excitation, ionization, and dissociation of atmospheric species by electrons is needed [15]. Reliable data on the e$^\pm$−CO$_2$ collision are, therefore, immensely necessary for controlling the atmospheric environment. Moreover, CO$_2$ is frequently used in gaseous discharges or low-temperature plasma devices.

In view of the wide applications of CO$_2$ described above, a number of experimental and theoretical studies of e$^\pm$−CO$_2$ scattering have been reported to date. Earlier investigations (up to the year 2001) on the e$^-$−CO$_2$ system have been compiled in review articles [14,16–19]. Among the recent studies on e$^-$−CO$_2$ scattering, absolute total ionization cross-sections (TICSs) were reported by Hudson et al. [20], who measured them at the threshold of 250 eV, and by Vinodkumar et al. [21], who calculated the threshold to be 5000 eV. In a later study, firstly, the total inelastic cross-section was calculated using the well-known spherical complex optical potential (SCOP) formalism. After that, the TICS was extracted by employing a semi-empirical formalism called the 'complex spherical potential-ionization contribution' (CSP-ic).

In contrast, positron scattering cross-sections for molecular targets have not been widely studied. However, for e$^+$−CO$_2$ systems, the literature shows a number of experimental and theoretical studies. For example, the TICS was measured by Laricchia and Moxom [22] at $E_i = 3$–20 eV, by Sueoka and Hamada [23] at 0.3–10 eV, by Bluhme et al. [24] at $E_i = $ threshold−2000 eV, and by Marler and Surko [25] at $E_i = $ threshold−90 eV. The measurement of the direct ionization cross-section was reported by Cooke et al. [26] in the energy range of 10–1000 eV. On the theoretical side, Baluja and Jain [27] employed a model of the complex optical potential to calculate the total (elastic + inelastic) cross-section (TCS) for a positron in the range of 1–5000 eV using several molecular targets, including CO$_2$. Campeanu et al. [28] predicted the same observable for $E_i = 20$–1000 eV using the CPE (Coulomb plus plane waves with full energy range) distorted wave model. Recently, Singh et al. [3] reported a TCS calculated over a wide energy range (threshold to 5000 eV) using a modified version of the SCOP.

Although extensive experimental and theoretical studies on e$^\pm$−CO$_2$ scattering have been performed, most of them only paid attention to the ionization processes. Data on other observables, e.g., the elastic differential cross-section (DCS), integrated elastic cross-section (IECS), inelastic cross-section (INCS), momentum-transfer cross-section (MTCS), viscosity cross-section (VCS), and total (elastic + inelastic) cross-section (TCS), are, therefore, too scarce in the literature. Moreover, the agreement between experiments and theories and even between various experiments is still unsatisfactory for practical purposes. To the best of our knowledge, for the e$^\pm$−CO$_2$ system, there is neither an experimental nor a theoretical calculation of the critical minima (CM) in the DCS that is available in the literature. The destructive interference of the scattered wave of different angular momentum states is responsible for such minima in the DCS. More studies of electron and positron collisions with this molecule are, therefore, immensely necessary to resolve the above problems. In particular, a reliable theoretical model can overcome the ambiguities in experimental measurements.

In the present work, we report our calculations of the DCS, TCS, IECS, INCS, MTCS, VCS, and TICS for both electron and positron scattering from a CO$_2$ molecule over a wider energy range of $1 \, \text{eV} \leq E_i \leq 1 \, \text{MeV}$. In addition, the spin polarization is evaluated for these scattering systems for the first time. In these calculations, we adopt a Dirac partial-wave analysis under the framework of a complex optical potential model (OPM). In order to make the partial-wave method effective for the projectile–molecule interaction, the present work uses a single-scattering independent atom model (IAM), as well as the IAM with screening correction (IAMS), which was first proposed by Blanco and Garcia [29] and then by Blanco et al. [30].

The IAMS approach [31] has already proven to be successful in calculating various observables for electron and positron scattering from a molecular carbon monoxide target. In this method, the target molecule is approximately replaced by its constituent atoms in the corresponding positions. The projectile–molecule interaction is thereby reduced to the projectile–atom interaction in the collision dynamics. It is worth mentioning that, under the optical potential framework, the present approaches (IAM and IAMS) do not require a fitting procedure; however, it is possible to vary one parameter ($\triangle$, the mean excitation energy of the target in the evaluation of absorption potential) in the calculation to bring the theory and experiments closer to each other. Nevertheless, the method is capable of predicting quite reliable cross-section data without adjusting the $\triangle$ parameter, and thus produces theoretical results where experimental data are not available.

2. Outline of the Theory

The scattering of electrons or positrons by a molecule cannot be treated straightforwardly with the procedure of partial waves due to the non-spherical nature of the above projectile–molecule interaction. In the additive rule (AR), the scattering cross-sections due to a molecule (differential or integrated) are obtained by simply adding the corresponding contributions due to the individual free atoms composing the molecule. This is an approximation that ignores the chemical bonding and aggregation effects. The density distribution of an atom in a molecule is different from that of the same atom in an isolated state. This distortion in the density distribution due to aggregation in the formation of the molecule changes the projectile–molecule interaction from a projectile–atom interaction and influences the scattering. In independent-atom approximation (IAM), the interaction of an atom in a molecule is transformed into that of a free atom, thus reducing the single-center scattering from a molecule into a multi-center scattering from a spherically symmetric potential due to a free atom. This approximation prepares the ground for the application of partial-wave analysis of scattering. In this approach, the molecular effect is taken into account by determining the differential cross-section (DCS) as the coherent sum of the waves (not the currents) scattered from the atoms, which are located in fixed positions in the molecule. Additionally, the first excitation energy and dipole polarizability of the molecule, instead of the atom, are used in generating the projectile–atom.

2.1. Relativistic Dirac Equation

The relativistic Dirac equation [32] for a projectile of resting mass m_o traveling in a central field $V(r)$ with a velocity v is given by

$$[c\alpha.p + \beta m_o c^2 + V(r)]\psi(\mathbf{r}) = E\psi(\mathbf{r}), \tag{1}$$

where $E = \gamma m_o c^2 = E_i + m_o c^2$ is the total energy, $\gamma = (1 - v^2/c^2)^{-1/2}$, c is the velocity of light in vacuum, E_i is the kinetic energy of the incident particle, and α and β are the usual 4×4 Dirac matrices.

2.2. Complex Optical Potential

The above Dirac equation is solved numerically by using the RADIAL subroutine package [33] and by employing a complex optical potential [34] of the following form:

$$\begin{aligned} V(r) &= V_{\text{real}}(r) - iW_{\text{abs}}(r) \\ &= V_{\text{st}}(r) + V_{\text{ex}}(r) + V_{\text{cp}}(r) - iW_{\text{abs}}(r). \end{aligned} \tag{2}$$

The real components $V_{\text{st}}(r)$, $V_{\text{ex}}(r)$, and $V_{\text{cp}}(r)$ represent the static, exchange, and correlation–polarization potentials, respectively, and the imaginary component, $W_{\text{abs}}(r)$ represents the magnitude of the absorption potential.

Static potential arises due to the electrostatic interaction between the projectile and the atomic charge distribution. This static potential is generated using the Dirac–Fock electron density [35] and Fermi nuclear charge distribution [36]. The exchange potential, $V_{\text{ex}}(r)$, for

electrons arises due to the indistinguishability of the incident and bound electrons of the target. For positrons, the exchange part is zero. The present study uses the semi-classical local exchange potential of Furness and McCarthy [37], which is derived from the non-local exchange interaction using the WKB-like wave functions. The polarization potential comes into effect due to the displacement of the charges of the atom by the incident charged projectile and remains attractive for both electrons and positrons. Following Salvat [38], this work employs a global correlation–polarization potential $V_{cp}(r)$, which combines the parameter-free long-range Buckingham potential and the short-range correlation potential based on local density approximation (LDA). The negative imaginary part, $-iW_{abs}(r)$, is included to account for the loss of particles into various inelastic channels that open beyond the inelastic threshold. The detailed shapes of components $V_{st}(r)$, $V_{ex}(r)$, $V_{cp}(r)$, and $W_{abs}(r)$ are given elsewhere [6,31,39].

In the Dirac partial-wave analysis, the scattering of electrons and positrons by the potential $V(r)$ is completely described by the elastic scattering amplitude [11]. It consists of a spin-conserving (direct) contribution $f(\theta)$ and a spin-flip contribution $g(\theta)$. The elastic DCS for an initially unpolarized electron/positron is obtained from

$$\frac{d\sigma}{d\Omega} = \mid f(\theta) \mid^2 + \mid g(\theta) \mid^2 \tag{3}$$

2.3. IAM Approach

As the projectile–molecule interaction is not spherically symmetric, the partial-wave method cannot be directly applied for the generation of observable quantities for $e^{\pm}-CO_2$ scattering. In the present IAM approach, the direct and spin-flip scattering amplitudes are, respectively, given by [31]:

$$F(\theta) = \sum_i \exp(i\mathbf{q}.\mathbf{r}_i) f_i(\theta) \tag{4}$$

and

$$G(\theta) = \sum_i \exp(i\mathbf{q}.\mathbf{r}_i) g_i(\theta) \tag{5}$$

where $\hbar\mathbf{q}$ is the momentum transfer, $\mathbf{r}_i$ is the position vector for the nucleus of the i-th atom relative to an arbitrary origin, and $f_i(\theta)$ and $g_i(\theta)$ are the scattering amplitudes for the constituent-free atom of an element. The corresponding DCS is then obtained by averaging the orientations of all of the randomly oriented molecules and is given by:

$$\frac{d\sigma}{d\Omega} = \langle |F(\theta)|^2 + |G(\theta)|^2 \rangle \tag{6}$$

$$= \sum_{i,j} \exp(i\mathbf{q}.\mathbf{r}_{ij})[f_i(\theta)f_j^*(\theta) + g_i(\theta)g_j^*(\theta)] \tag{7}$$

$$= \sum_{i,j} \frac{\sin(qr_{ij})}{qr_{ij}}[f_i(\theta)f_j^*(\theta) + g_i(\theta)g_j^*(\theta)] \tag{8}$$

$$= \sum_i [|f_i(\theta)|^2 + |g_i(\theta)|^2] + \sum_{i \neq j} \frac{\sin(qr_{ij})}{qr_{ij}}[f_i(\theta)f_j^*(\theta) + g_i(\theta)g_j^*(\theta)] \tag{9}$$

Here, $q = 2k\sin(\theta/2)$, r_{ij} is the distance between the i-th and j-th atoms, $\sin(qr_{ij})/qr_{ij} = 1$ when $qr_{ij} = 0$, and the term $\sum_{i \neq j}$ represents the contribution of interference to the molecular DCS.

In terms of the DCS, the integrated elastic σ_{el}, momentum-transfer σ_m, and viscosity σ_v cross-sections for the $e^{\pm}-CO_2$ scattering are expressed as

$$\sigma_{el} = \int \frac{d\sigma}{d\Omega} d\Omega = 2\pi \int_0^{\pi} \left(\frac{d\sigma}{d\Omega}\right) \sin(\theta) d\theta \tag{10}$$

$$\sigma_{\mathrm{m}} = 2\pi \int_0^\pi (1 - \cos\theta)\left(\frac{d\sigma}{d\Omega}\right) sin(\theta) d\theta \tag{11}$$

$$\sigma_{\mathrm{v}} = 3\pi \int_0^\pi \left[1 - (\cos\theta)^2\right]\left(\frac{d\sigma}{d\Omega}\right) sin(\theta) d\theta \tag{12}$$

The total cross-section σ_{tot} for both of the projectiles can be obtained from the following expression:

$$\sigma_{\mathrm{tot}} = \frac{4\pi}{k} \sum_i \mathrm{Im} f_i(0), \tag{13}$$

where $\mathrm{Im} f_i(0)$ denotes the imaginary part of the direct scattering amplitude in the forward direction at $\theta = 0°$ for the i-th atom. Because of the imaginary component, σ_{tot} contains both the elastic and inelastic (absorption) parts. In the present study, the inelastic cross-section σ_{in} is expressed as

$$\sigma_{\mathrm{inel}} = \sigma_{\mathrm{tot}} - \sigma_{\mathrm{el}} \tag{14}$$

2.4. IAMS Approach

The main drawback of the IAM model that it does not consider multiple scattering of projectiles from the constituent atoms of a molecule, making it applicable only at comparatively high energies ($>$100 eV) [30,31]. Another reason for the low-energy failure of this model is its ignorance of the mutual overlapping of nearby atomic cross-sections. To overcome this problem, Blanco and Garcia [29] proposed a screening that corrected s_i ($0 \leq s_i \leq 1$) for i-th and j-th atoms of a molecule, which are given by:

$$s_i = 1 - \frac{\varepsilon_i^{(2)}}{2!} + \frac{\varepsilon_i^{(3)}}{3!} - \frac{\varepsilon_i^{(4)}}{4!} + \ldots \pm \frac{\varepsilon_i^{(N)}}{N!} \tag{15}$$

where

$$\varepsilon_i^{(m)} = \frac{N - m + 1}{N - 1} \sum_{i \neq j} \frac{\sigma_j \varepsilon_j^{(m-1)}}{\alpha_{ij}} \quad (m = 2, \ldots, N). \tag{16}$$

represents m-atoms overlapping. N is the number of atoms in the target molecule and $\alpha_{ij} = max(4\pi r_{ij}^2, \sigma_i, \sigma_j)$, where σ_i and σ_j are the atomic total cross-sections for the i-th and j-th atoms of the molecule. For a CO_2 molecule ($N = 3$), Equation (15) takes the following form:

$$s_i = 1 - \frac{\varepsilon_i^{(2)}}{2!} + \frac{\varepsilon_i^{(3)}}{3!} \tag{17}$$

These coefficients s_i reduce the contributions of constituent atoms to the molecular cross-section. Blanco et al. [30] improved the formalism by adding another factor, v_{ij}, to the positive values of $\sum_{i \neq j} v_{ij} s_i s_j \frac{\sin(q r_{ij})}{q r_{ij}}[f_i(\theta) f_j^*(\theta)]$, which is defined as $v_{ij} = r_{ij}^2/(r_{ij}^2 + \rho_{ij}^2)$, with a length-dimensional parameter $\rho_{ij} = max(\sqrt{\sigma_i/\pi}, \sqrt{\sigma_j/\pi}, 1/k)$. Here, $(\sqrt{\sigma/\pi})$ represents the radius of a circle of area σ. So, the screening-corrected version of Equation (9) is

$$\left(\frac{d\sigma}{d\Omega}\right)^s = \sum_i s_i^2[|f_i(\theta)|^2 + |g_i(\theta)|^2]$$
$$+ \sum_{i \neq j} v_{ij} s_i s_j \frac{\sin(q r_{ij})}{q r_{ij}}[f_i(\theta) f_j^*(\theta) + g_i(\theta) g_j^*(\theta)] \tag{18}$$

The screening-corrected integrated elastic σ_{el}^s, momentum-transfer σ_{m}^s, viscosity σ_{v}^s, and total σ_{tot}^s cross-sections are given by

$$\sigma_{\text{el}}^s = 2\pi \int_0^\pi \left(\frac{d\sigma}{d\Omega}\right)^s \sin(\theta)d\theta \tag{19}$$

$$\sigma_{\text{m}}^s = 2\pi \int_0^\pi (1 - \cos\theta)\left(\frac{d\sigma}{d\Omega}\right)^s \sin(\theta)d\theta \tag{20}$$

$$\sigma_{\text{v}}^s = 3\pi \int_0^\pi \left[1 - (\cos\theta)^2\right]\left(\frac{d\sigma}{d\Omega}\right)^s \sin(\theta)d\theta \tag{21}$$

$$\sigma_{\text{tot}}^s = \sigma_{\text{el}}^s + \sigma_{\text{inel}}^s = \sum_i s_i(\sigma_{\text{el}} + \sigma_{\text{inel}}) = \sum_i s_i \sigma_{\text{tot}} \tag{22}$$

The spin polarization of a randomly oriented molecule in terms of the scattering amplitudes is expressed as

$$S(\theta) = i\frac{\langle F(\theta)G^*(\theta) - F^*(\theta)G(\theta)\rangle}{\langle |F(\theta)|^2 + |G(\theta)|^2 \rangle} \tag{23}$$

The interaction energy of the polarizing field with the CO_2 molecule vanishes to the first approximation. However, for a large projectile–atom distance , the polarizability of the i-th atom of the molecule, the response to the polarizing field, is approximately equal to the polarizability of the free atom multiplied by the ratio of the molecular polarizability to the sum of the polarizabilities of the atoms composing the molecule. This way, a molecular feature enters into the expression for the projectile–atom polarization potential. For the calculations of scattering amplitudes from the i-th atom, we used the following formula for effective polarizability:

$$\alpha_{d,eff}(i) = \alpha_d^{mol}\alpha_d(i)\left[\sum_j \alpha_d(j)\right]^{-1}. \tag{24}$$

Here, the summation extends over all of the constituent atoms in the molecule. The atomic polarizabilities for carbon and oxygen are used: 1.76Å^3 [40] and 0.802Å^3 [40], respectively. The molecular polarizability of the CO_2 molecule is 2.507Å^3 [41]. In the independent atom model approximation, the effective atomic polarizability defined by Equation (24) is used to calculate the polarization potential $V_p(r)$ for an atom. The values of first molecular excitation energy and ionization potential are 11.04 eV [3] and 13.773 eV [42] for the present analysis.

Since the inelastic channels in $e^\pm-$molecule scattering consist of both excitation and ionization, the total inelastic cross-section σ_{inel} in Equation (14) can be further divided into an excitation (σ_{ex}) and an ionization (σ_{ion}) part as follows:

$$\sigma_{\text{inel}} = \sigma_{\text{ex}} + \sigma_{\text{ion}}. \tag{25}$$

Therefore, σ_{inel} and σ_{ion} satisfy the following inequality:

$$\sigma_{\text{inel}} \geq \sigma_{\text{ion}}. \tag{26}$$

In the present study, the total ionization cross-section (σ_{ion}) is calculated from the following energy-dependent ratio [43,44]:

$$R(E_i) = \frac{\sigma_{\text{ion}}(E_i)}{\sigma_{\text{inel}}(E_i)}, \tag{27}$$

with $0 \leq R \leq 1$.

The ratio $R(E_i)$ is a continuous function of energy. For $E_i > I$ (ionization potential), this function is fitted to the equation

$$R(E_i) = 1 - B_1\left[\frac{B_2}{U+C} + \frac{\ln U}{U}\right] \tag{28}$$

where $U = E_i / I$ is the reduced energy. It was observed experimentally that the value of $R(E_i)$ rises steadily as the energy increases above the threshold and approaches unity at very high energies. The adjustable parameters B_1, B_2, and C are, therefore, determined using the following conditions:

$$R(E_i) = \begin{cases} 0 & \text{for } E_i \leq I, \\ R_p & \text{for } E_i = E_p \\ R_F & \text{for } E_i \geq E_F > E_P. \end{cases} \tag{29}$$

Here, R_p is the value of R at $E_i = E_p$, with E_p being the incident energy at which the maximum absorption occurs. At incident energies $E_i \geq E_F$, well above the peak position E_p, the value of R increases to R_F (very close to 1). The optimal values of the parameters B_1, B_2, and C obtained from the solutions of Equations (29) using a FORTRAN program are, respectively, found to be -1.263, -5.886, and 6.436 both for electron and positron scattering.

3. Results and Discussion

In the present study, the ELSEPA code [34] was used for the calculation of various scattering observables for $e^{\pm} - CO_2$ scattering systems over a wide energy range. The differential and total cross-sections for both of the projectiles (electron and positron) were calculated for the energy domain of 1 eV $\leq E_i \leq 1$ MeV. The Sherman function was calculated for the energy range of 5–1500 eV. The program first calculated the phase shifts δ_k required for the calculations of scattering amplitudes from the solutions of the Dirac equation up to a matching distance and then for matching with the known exterior solution. The program then calculated, using the knowledge of the scattering amplitudes, various scattering observables for spin-unpolarized electrons or positrons. In this section, we present the results and analyses of several scattering observables that were calculated with both our IAM and IAMS approaches.

3.1. The Differential Cross-Section

Figures 1–4 display the DCS results for electrons that are elastically scattered from a carbon dioxide molecule, as calculated by our two approaches over the energy range of 40 eV $\leq E_i \leq 10$ keV. As seen in these figures, the IAMS approach produces reduced values of DCS compared to those obtained with the IAM approach, especially at lower energies and angles, which is consistent with experimental observations. This important feature signifies that the inclusion of the screening effect makes the IAMS theory effective in describing the DCS of $e^- - CO_2$ scattering. One can also notice, as expected, that at higher energies, both the IAM and IAMS give almost the same results. At these energies, the corresponding de Broglie wavelengths of the projectile are small enough compared to the inter-atomic distances of the target molecules. Incident particles, therefore, participate in the collision with all of the atoms (inside the target molecule) independently, without any kind of geometrical overlapping among them.

The oscillations of the DCS with the angle (or energy) are interference structures that are seen only in lower-energy domains (well below 1000 eV). These structures are of great interest for the study of collision dynamics, as they appear due to the diffraction effects arising from the quantum-mechanical nature of matter. The interference structures disappear when the collision becomes so energetic that the projectile–atom interactions occur inside the K-shell. However, these diffraction minima differ in number between our two approaches (IAM and IAMS). The number of minima predicted by the IAM theory varies with energy from 1 at $E_i = 40$ eV to 2 at $80 \leq E_i \leq 600$ eV, and then reduces to 1 at $700 \leq E_i \leq 1000$ eV. At energies greater than 1000 eV, the structure vanishes due to the incoherent interference of the scattered waves of many angular momenta. The IAMS theory, on the other hand, produces only one minimum up to $E_i = 200$ eV, and beyond that, the DCS shows smooth variation with the energy.
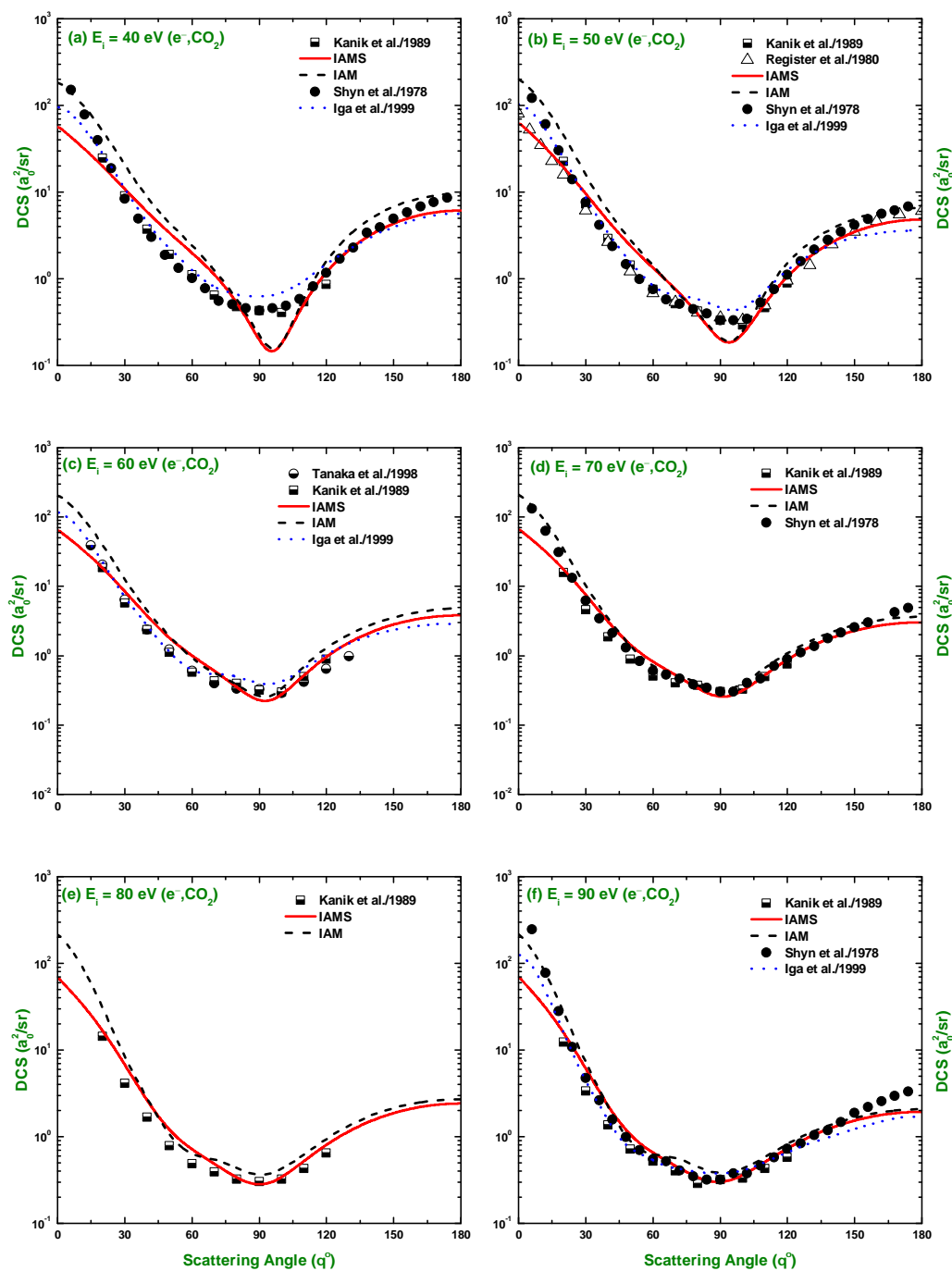
Figure 1. DCS (a_0^2/sr) for the elastic scattering of electrons from carbon dioxide at energies of 40, 50, 60, 70, 80, and 90 eV. Theoretical: IAM, IAMS, and Iga et al. [45]. Experimental: Tanaka et al. [46], Shyn et al. [47], Register et al. [48], and Kanik et al. [49].

In Figures 1–4, our DCS results for the electron projectiles are compared with the experimental data from Tanaka et al. [46] that are available at E_i = 60–100 eV, as well as those of Shyn et al. [47] at E_i = 40–90 eV, Register et al. [48] at 50 eV, Kanik et al. [49] at E_i = 40–100 eV, Iga et al. [45] at 100, 200, 300, and 400 eV, Bromberg [50] at 300, 400, and 500 eV, Maji et al. [51] at 500, 700, and 900 eV, and Iga et al. [52] at 500, 800, and 1000 eV. For comparison, the experimental data of [47] are normalized with those of [49] in Figure 1 at 90°. Additionally included are the theoretical results predicted by the Schwinger variational iterative method (SVIM) of Iga et al. [45] at 100, 200, 300, and 400 eV and the IAM approach of Maji et al. [51] at 500, 700, and 900 eV. We found no experimental or any

other theoretical results with which to compare our calculations for the energy domain of $1500 \text{ eV} \leq E_i \leq 10{,}000 \text{ eV}$.
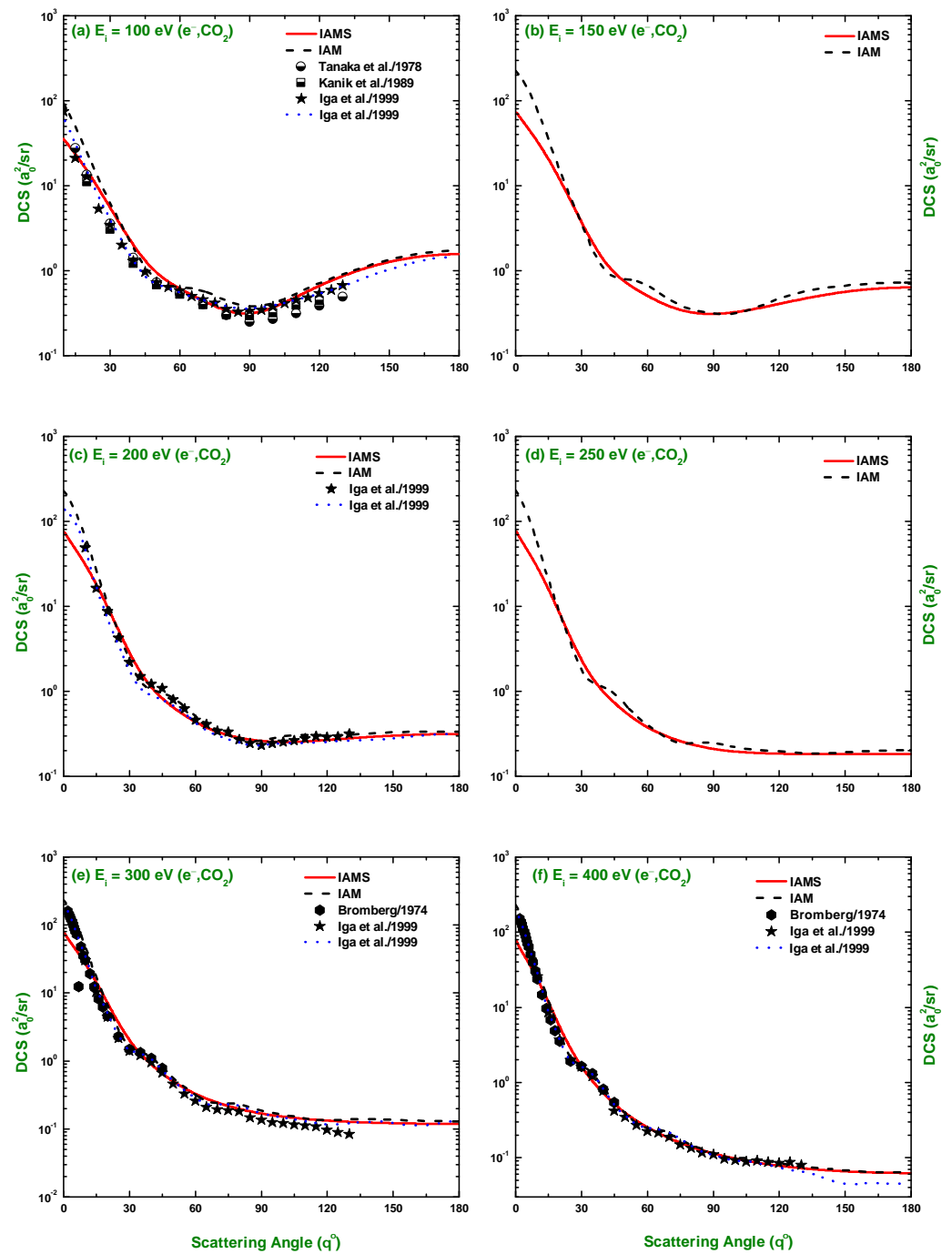
Figure 2. DCS (a_0^2/sr) for the elastic scattering of electrons from carbon dioxide at energies of 100, 150, 200, 250, 300, and 400 eV. Theoretical: References in Figure 1. Experimental: References in Figure 1, Iga et al. [45], and Bromberg [50].
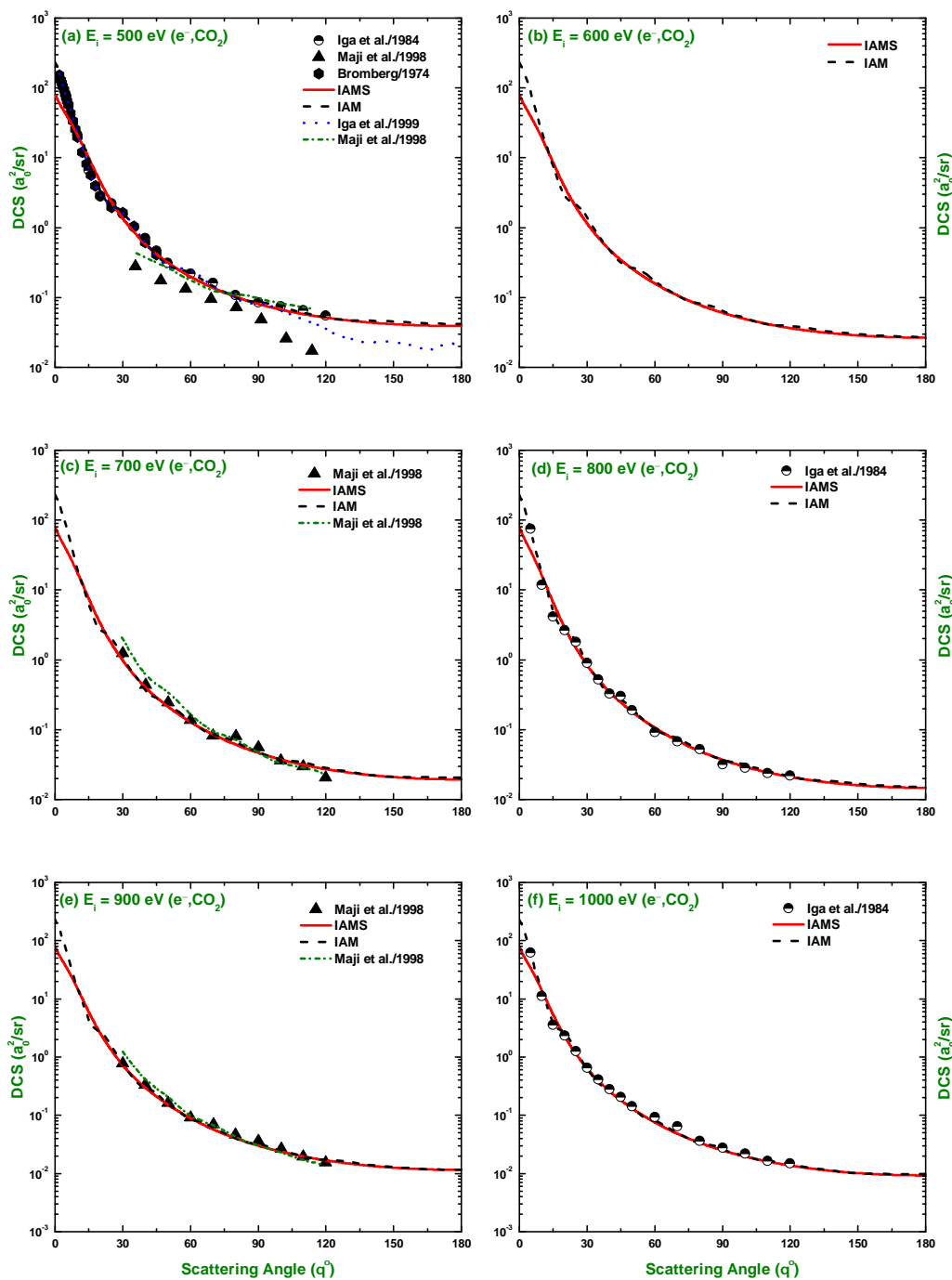
Figure 3. DCS (a_0^2/sr) for the elastic scattering of electrons from carbon dioxide at energies of 500, 600, 700, 800, 900, and 1000 eV. Theoretical: References in Figure 1. Experimental: References in Figures 1 and 2 and Maji et al. [51].

The comparison shows that our DCS results predicted by both of the approaches produce a reasonable agreement with the experimental data for $E_i \geq 60$ eV, except with the data of Maji et al. [51] at 500 eV. The present results, the experimental data, and the other theoretical values exhibit oscillations at about the same scattering angles. However, at the particular energy of 500 eV, the data of [51] differ from those of other experiments and theories, and even from their own calculations. At lower energies, especially at $E_i \leq 50$ eV, our results show noticeable disagreement with the results of the experiments, although they agree in terms of the number of minima with differences in magnitudes. This low-energy behavior can be treated properly by more sophisticated theories, such as the R-matrix,

convergent-close-coupling procedures, etc. The present OPM theory does not work well at low energies owing to the approximation from coupled-channel theory.
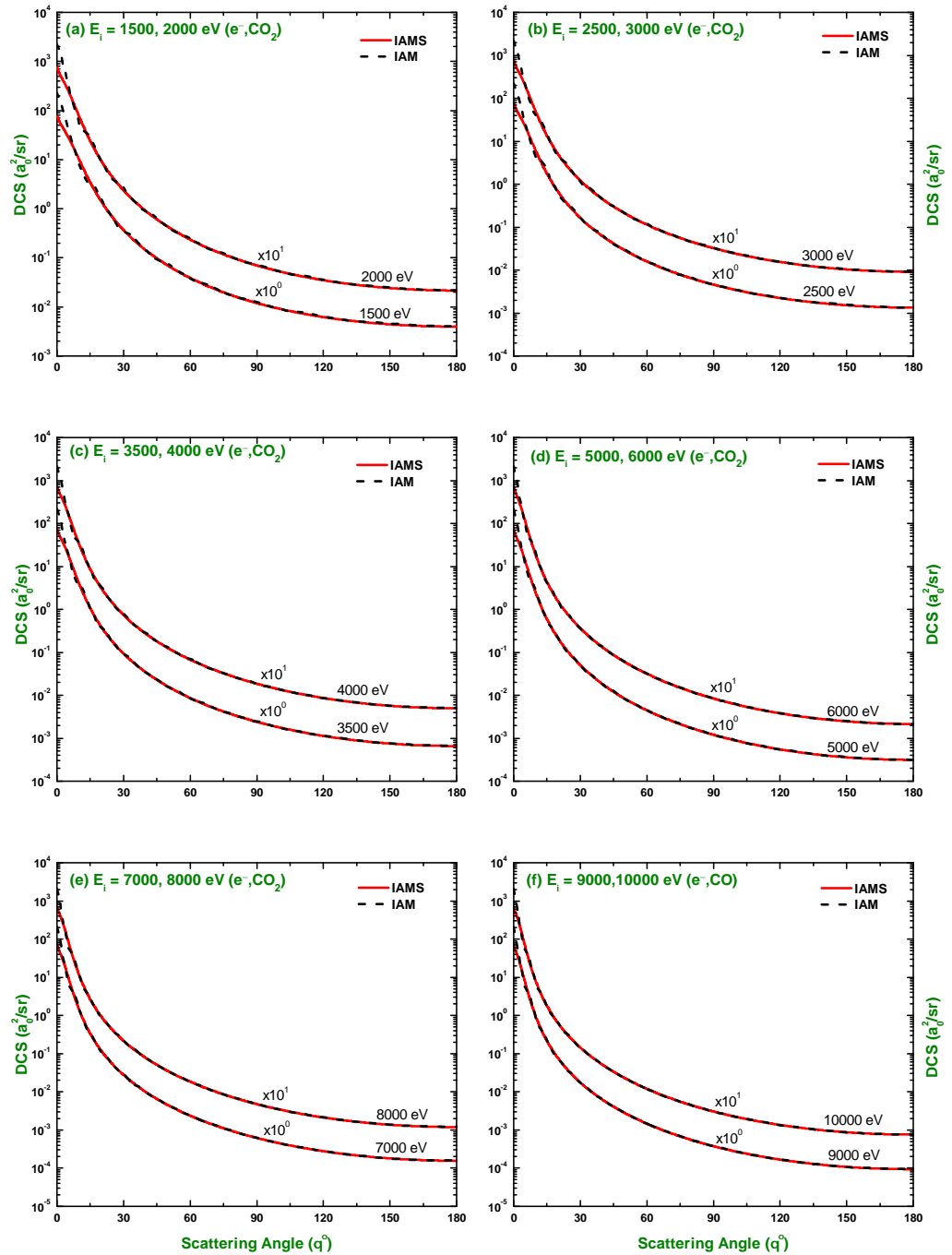
Figure 4. DCS (a_0^2/sr) for the elastic scattering of electrons from carbon dioxide at energies of 1500, 2000, 2500, 3000, 3500, 4000, 5000, 6000, 7000, 8000, 9000, and 10,000 eV. Theoretical: IAM and IAMS.

Figures 5–7 display our DCS results for the positron projectiles in the energy range of $20 \, \text{eV} \leq E_i \leq 10 \, \text{keV}$. As seen in these figures, the reduction of screening-corrected DCSs at lower scattering angles and energies is similar to that of their electron counterparts. Our results are compared with the experiments of Przybyla et al. [53] in Figure 5 at $E_i = 10, 20, 50,$ and 100 eV. For comparison, the experimentally measured data of [53] are normalized with our calculations (IAMS) at $105°$. As for the electron projectiles, at lower energies ($E_i \leq 20 \, \text{eV}$), in Figure 5, we observe significant discrepancies in magnitude and fair con-

cordance in the pattern of our calculations with the data. However, the quality of fit of our results to the data improves beyond 20 eV. Some reasons for the disagreement in the low-energy region of our calculations with the measured values have already been mentioned in the discussion of the electron scattering results. Another reason might be argued that the scattering data for positrons are not purely elastic, rather quasi-elastic [53]. These data have elastically scattered and rotational or vibrational excitations and have significant contributions to elastic scattering in the low-energy region, but lesser contributions in the high-energy region.

Our DCS calculations for positron scattering are also compared with those of Dapor and Miotello [54] in Figures 6 and 7, which are available at 500, 1000, 1500, 2000, 2500, 3000, 3500, and 4000 eV. It is to be noted that the $e^+ - CO_2$ scattering data of Dapor and Miotello [54] were produced by applying the AR to their positron–atom scattering cross-sections of C and O atoms. Following the same procedure, we also generated the IECS, MTCS, and VCS data of [54] and presented them in Figure 17c,e,f for comparison. One can see a close agreement of our calculations with those of [54] in shape (in the case of DCS), but slight differences in magnitude (in the case of DCS, IECS, MTCS, and VCS). However, the difference gradually decreases with increasing impact energy, and the results of [54] almost merge with those of both of our approaches (IAM and IAMS), implying that, in the high-energy region, the structural effect does not arise, and the individual atoms act independently owing to the low de Broglie wavelength of the incident projectile. The projectile–molecule interaction is predominantly a projectile–atom interaction.
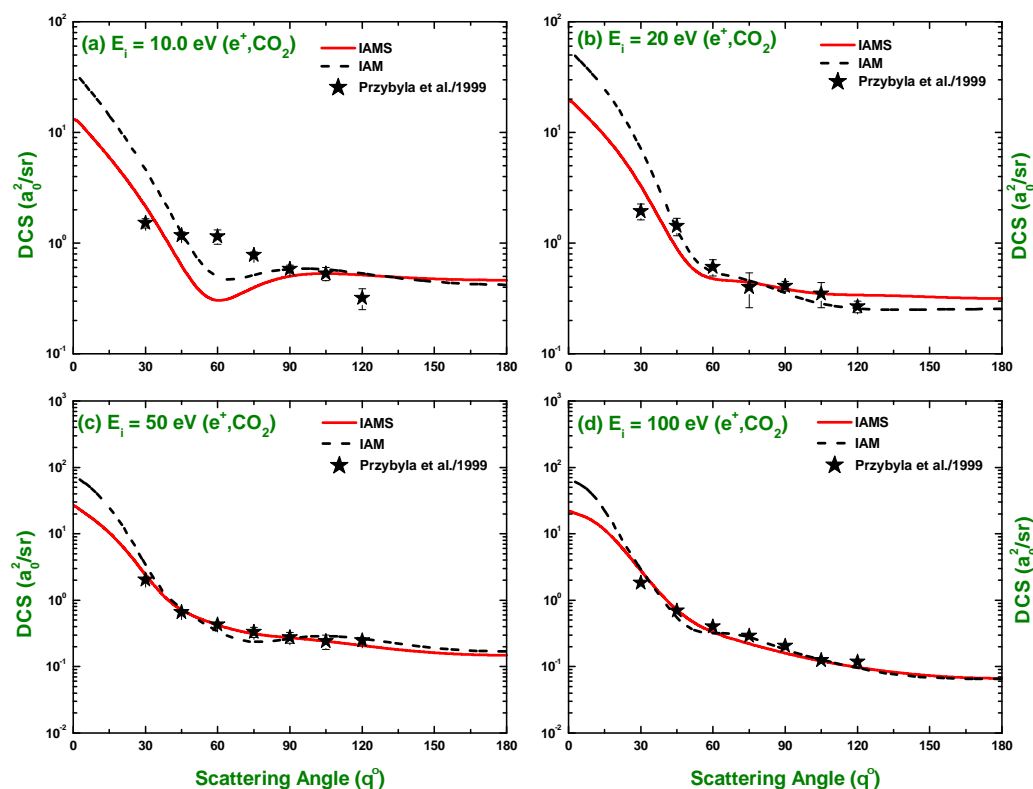
Figure 5. DCS (a_0^2/sr) for the elastic scattering of positrons from carbon dioxide at energies of 10, 20, 50, and 100 eV. Theoretical: IAM and IAMS. Experimental: Przybyla et al. [53].
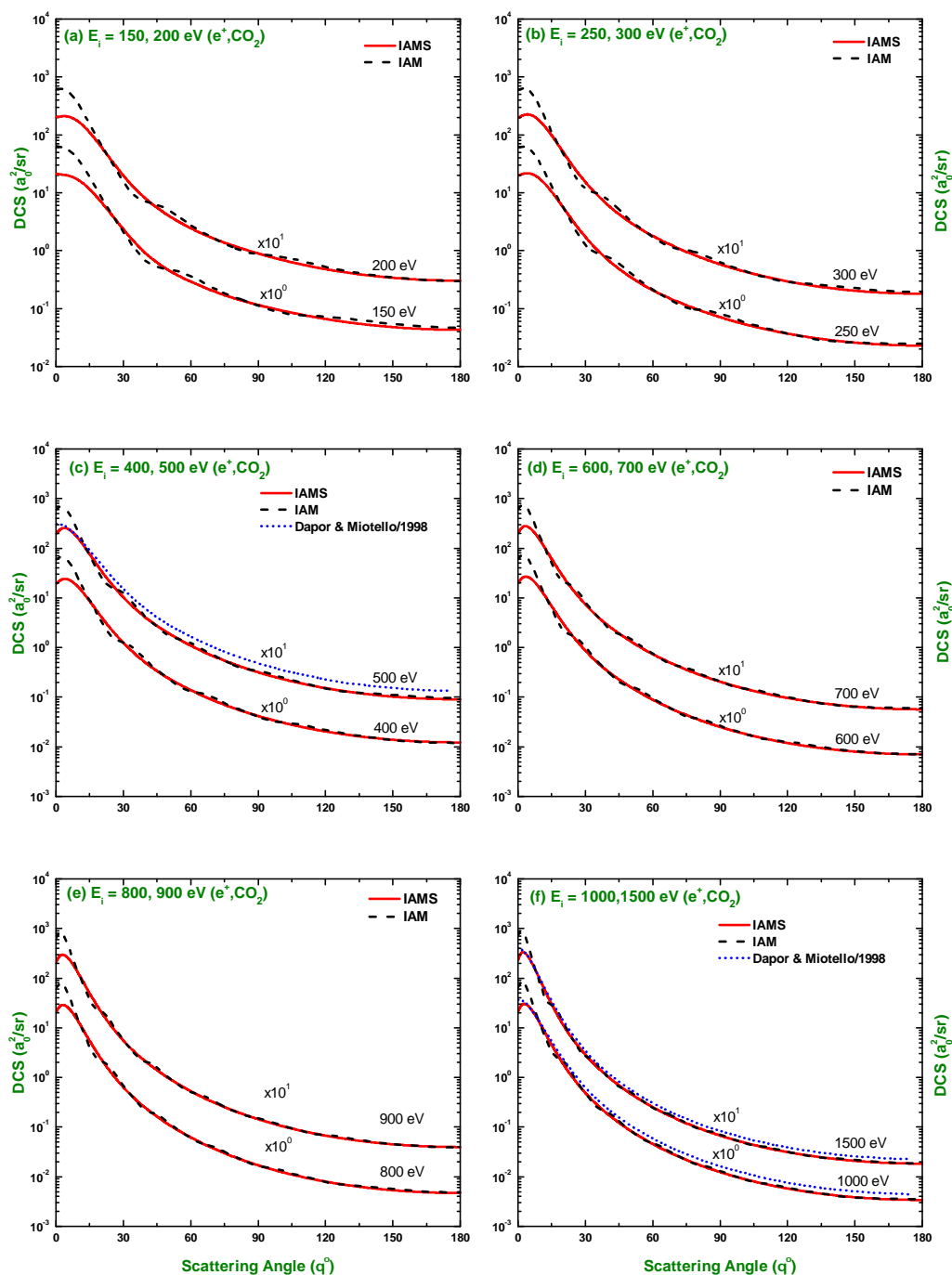
Figure 6. DCS (a_0^2/sr) for the elastic scattering of positrons from carbon dioxide at energies of 150, 200, 250, 300, 400, 500, 600, 700, 800, 900, 1000, and 1500 eV. Theoretical: IAM, IAMS, and Dapor and Miotello [54].

Figures 8 and 9, which are, respectively, for the electron and positron projectiles, depict the variation of the DCS with energy at angles $\theta = 30°$, $60°$, $90°$, and $120°$. As seen in these figures, the DCS minima, sharp or flat, occur up to around 200 eV, but disappear at higher energies. It is to be noted that a minimum in the DCS is formed due to destructive interference of waves scattered from bound electrons. At higher energies, the structure disappears in the DCS and leads to a monotonous pattern of the DCS due to the short interaction time, preventing the interference of scattered waves.
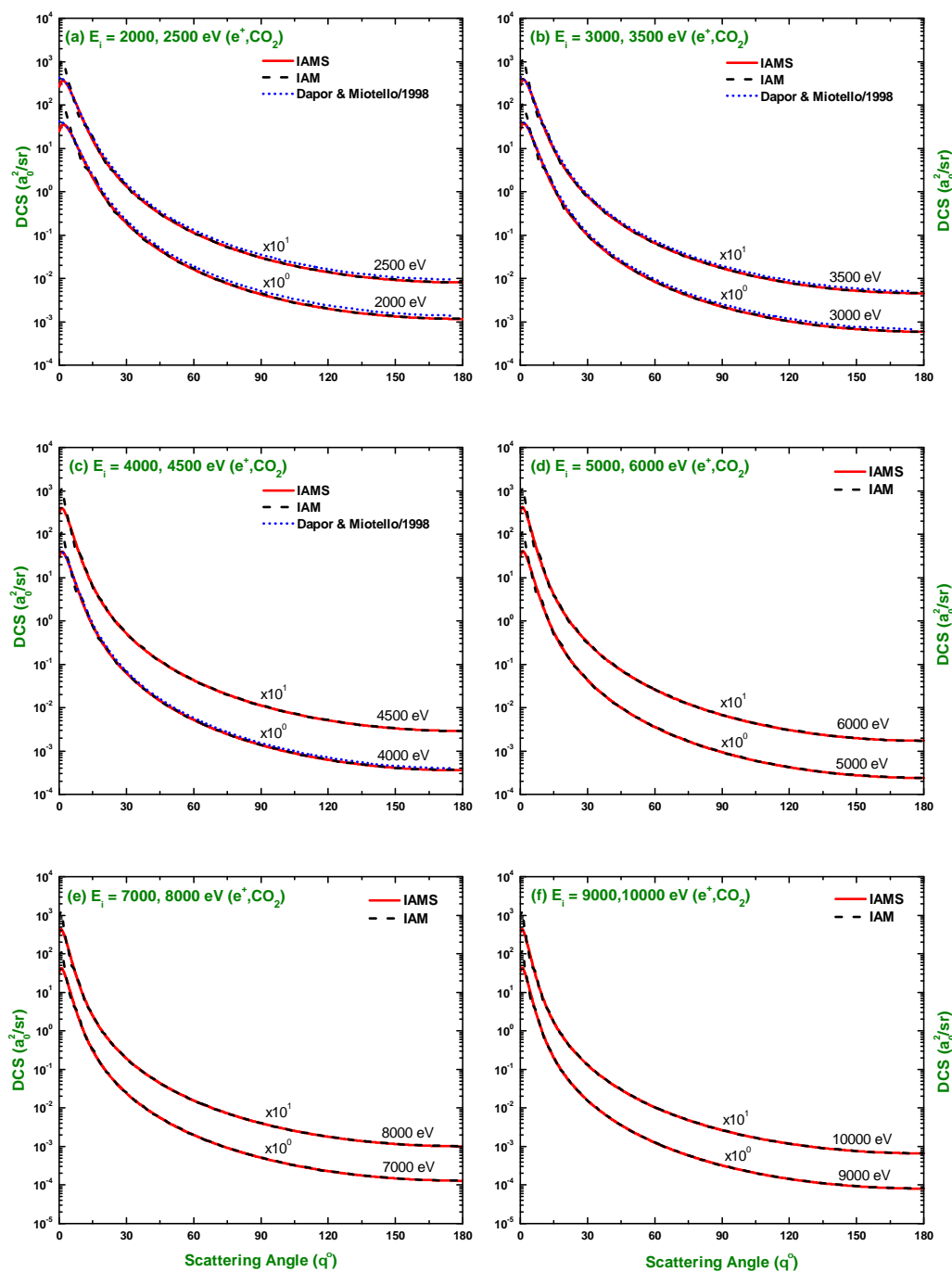
Figure 7. DCS (a_0^2/sr) for the elastic scattering of positrons from carbon dioxide at energies of 2000, 2500, 3000, 3500, 4000, 4500, 5000, 6000, 7000, 8000, 9000, and 10,000 eV. References in Figure 6.

The DCSs for electron scattering in Figure 8 are compared with the experiments of [45–52], and it was found that our results closely agree, at all angles, with the whole experimental data range, except at $E_i \leq 20$ eV. The same scenario is observed in Figure 9 for the positron scattering. One can also observe that the experimental cross-sections of electron scattering show a larger spread among different datasets at some energies, signifying that a theoretical method is very essential for the removal of the discrepancies and can be used as the recommended set of cross-sections.
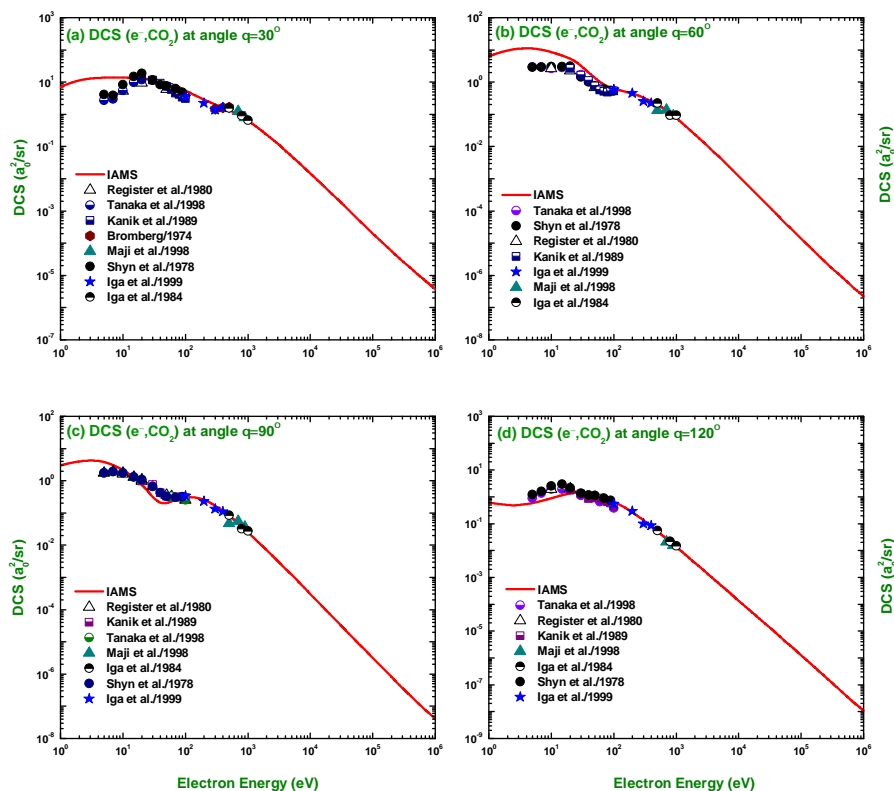
Figure 8. Energy dependence of the DCS (a_0^2/sr) for the elastic scattering of electrons from carbon dioxide at angles of 30°, 60°, 90°, and 120°. References: available in Figures 1–4.
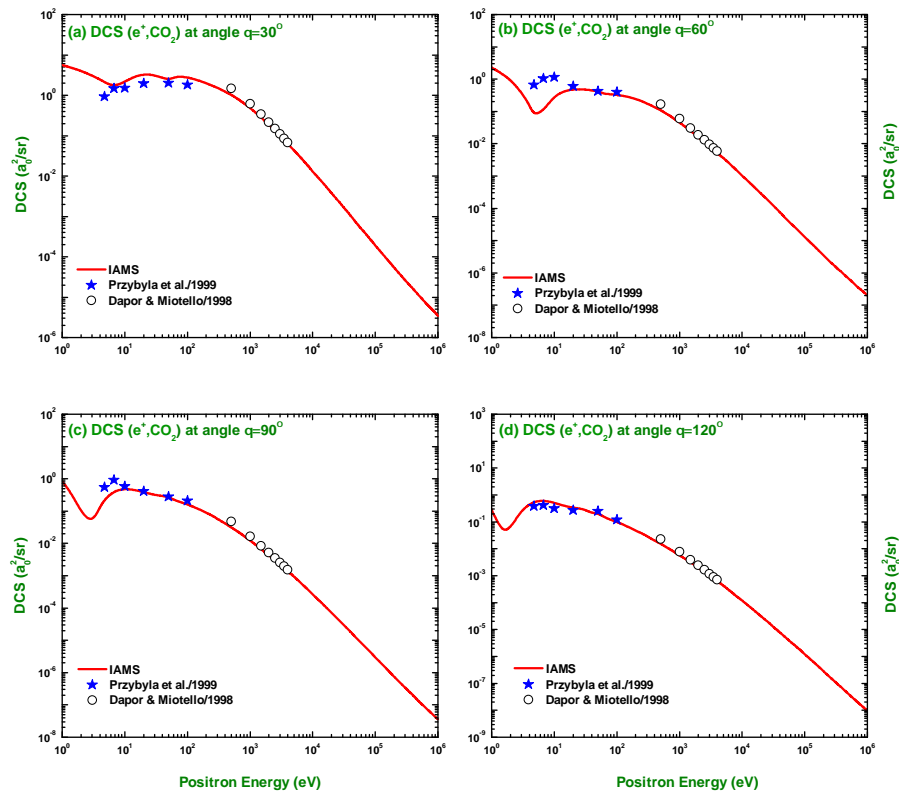
Figure 9. Energy dependence of the DCS (a_0^2/sr) for the elastic scattering of positrons from carbon dioxide at angles of 30°, 60°, 90°, and 120°. References: available in Figures 5–7.

Figure 10 displays the DCSs for the impact of electrons and positrons at the four angles of $30°$, $60°$, $90°$, and $150°$ as a function of collision energy. This comparison shows that, for both of the projectiles, the dependence on the incident energy is the same for higher energies beyond 10 keV. However, in the lower-energy region ($E_i \leq 10$ keV), the magnitude is smaller for positron scattering, indicating that the positron–molecule scattering is rather weaker than its electron counterpart due to the effect of exchange potential in the $e^- -$atom interaction. It is also observed that the positron DCSs start oscillating at a lower energy due to the difference in the correlation polarization potential.

The variation of the DCSs in terms of both collision energy and scattering angle is displayed in Figures 11 and 12, respectively, for electron and positron projectiles. These three-dimensional distributions of the DCS also confirm the disappearance of the interference structure in the DCS at higher energies because of the short duration of interaction between the projectile and molecule.
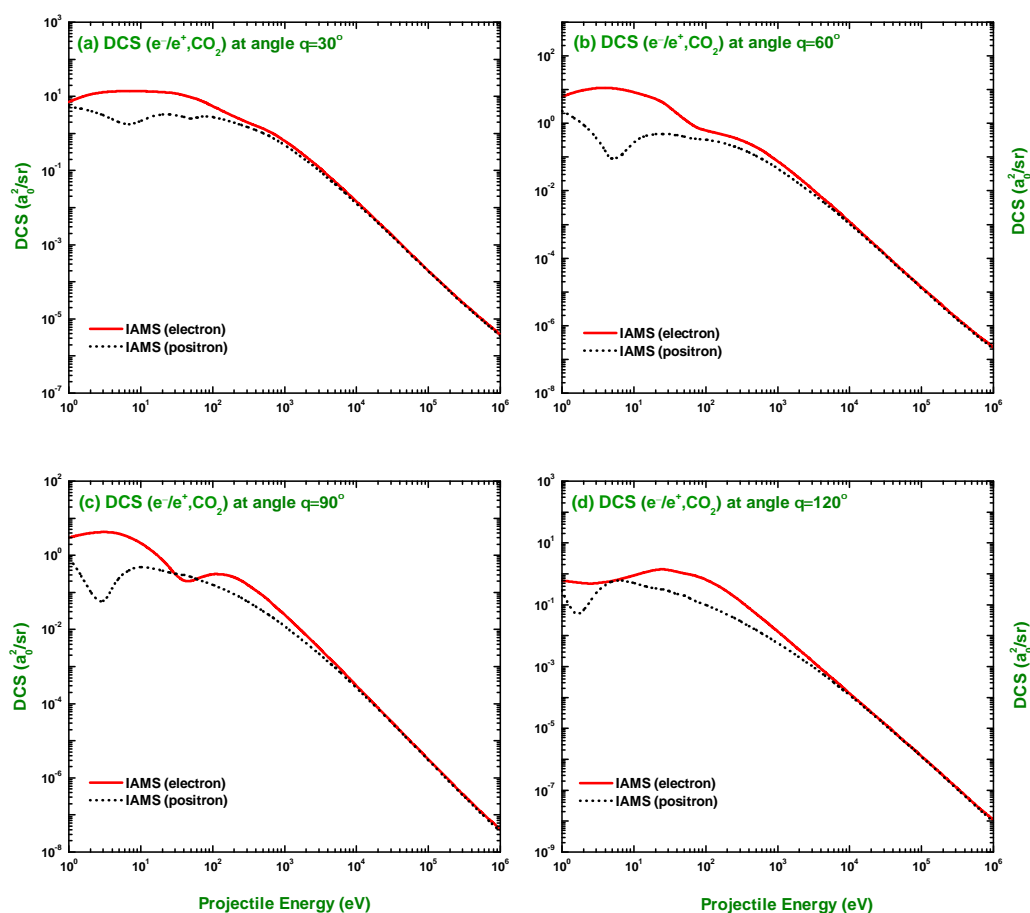
Figure 10. Comparison of the DCSs (a_0^2/sr) for the elastic scattering of electrons and positrons from carbon dioxide at angles of $30°$, $60°$, $90°$, and $120°$.
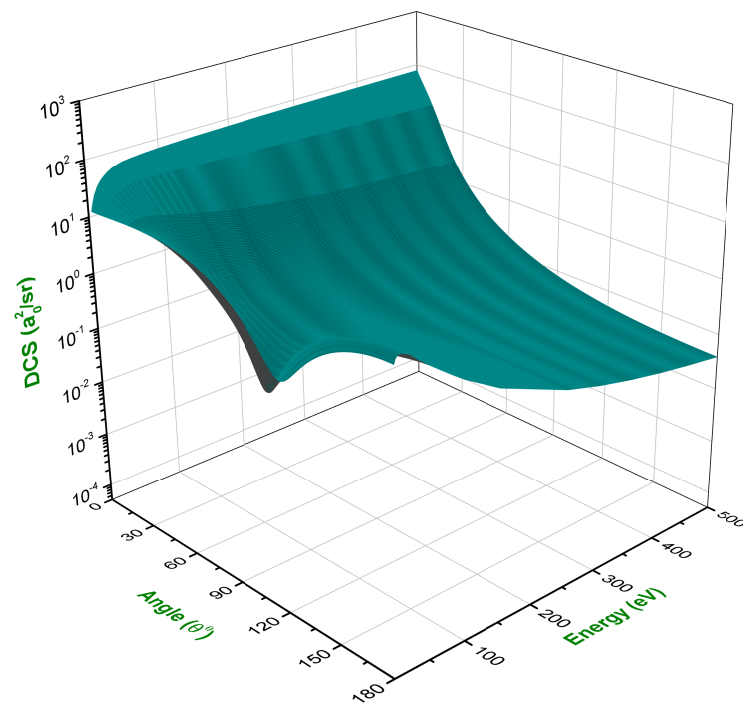
Figure 11. Variation of the DCS (a_0^2/sr) for the elastic scattering of electrons from carbon dioxide.
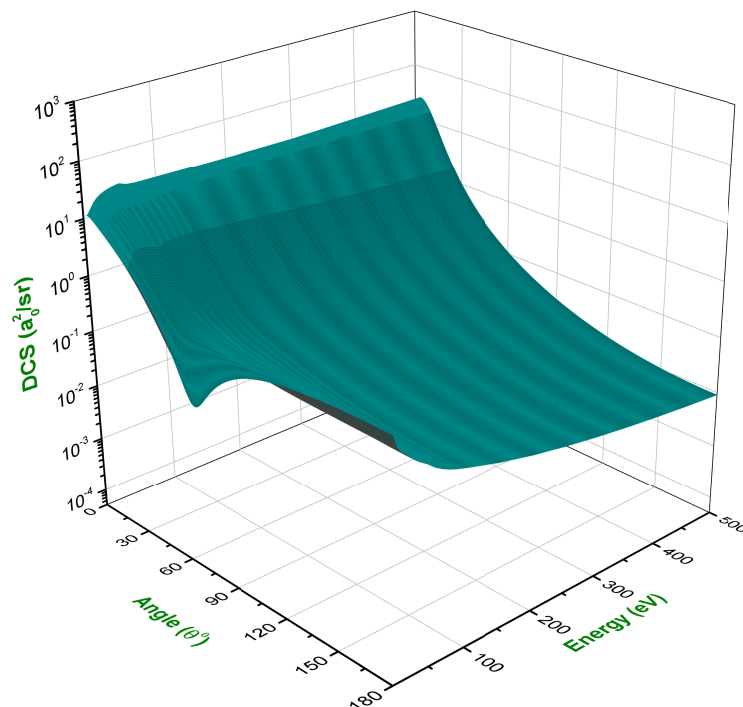
Figure 12. Variation of the DCS (a_0^2/sr) for the elastic scattering of positrons from carbon dioxide.

3.2. Sherman Function

In Figures 13 and 14, we present our IAM results of the Sherman function $S(\theta)$ for electrons that are elastically scattered from CO_2 molecules for incident energies of $5 \leq E_i \leq 1500$ eV. As seen in these figures, the minima in $S(\theta)$ relate to the minima in the DCS. In addition, as expected, the structures in $S(\theta)$ are much more pronounced because of the greater sensitivity of this observable to the variation in the potential as compared to the DCS.
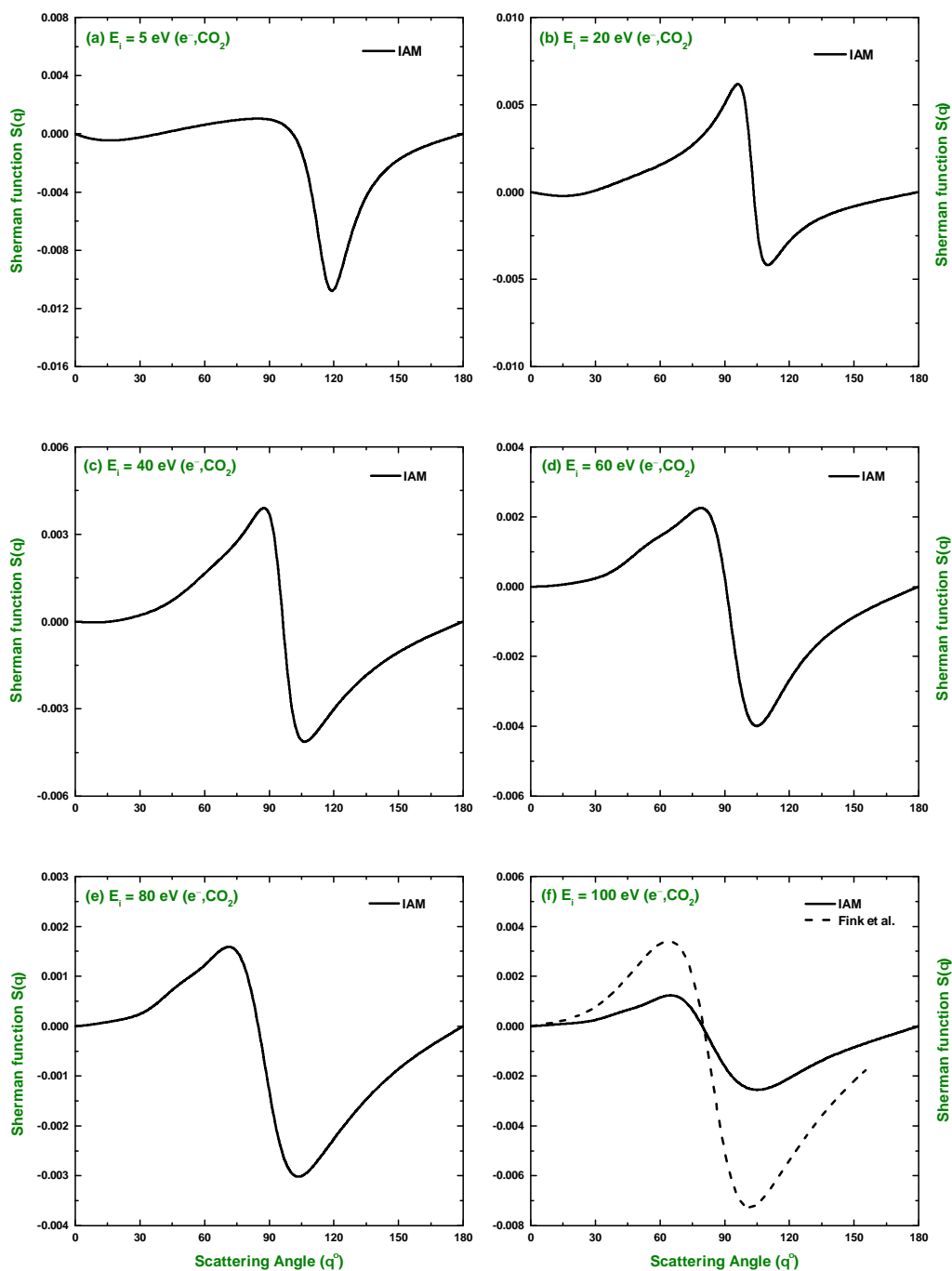
Figure 13. Angular dependence of the spin polarization of scattered electrons. Theoretical: IAM, Fink and Yates [55], and Fink and Ingram [56].

As far as we are aware, there are neither experimental nor any other theoretical spin polarization results for $e^- - CO_2$ scattering available in the literature. Fink and Yates [55] and Fink and Ingram [56] calculated $S(\theta)$, respectively, for carbon and oxygen atoms at energies of 100, 250, 500, 1000, and 1500 eV. By employing AR, we generated $S(\theta)$ for $e^- - CO_2$ at the aforementioned impact energies to compare with our calculations. It was observed that the comparison produces a fairly good agreement in pattern with differences in magnitude. This is not unexpected; as already mentioned, $S(\theta)$ is highly sensitive to variations in the procedure used to generate it.

Figure 15 shows the Sherman function for positron scattering due to our IAM theory at the collision energies of 4.75, 6.75, 10, 20, 50, and 100 eV. As is apparent in this figure,

at lower energies (<10 eV), our calculations produce only one maximum at each of these energies, which is shifted towards a lower scattering angle with increasing energy. Within the energy domain of $20 \leq E_i \leq 100$ eV, the Sherman function produces another maximum, which is shifted towards a higher scattering angle with increasing energy. Moreover, the spin asymmetry for positrons is extremely small, implying that the positron–molecule interaction is much weaker than in the case of electron impact because the spin polarization depends on the spin–orbit interaction, as well as on the spatial interaction potential. The lack of experimental and any other theoretical results precludes any comparisons.
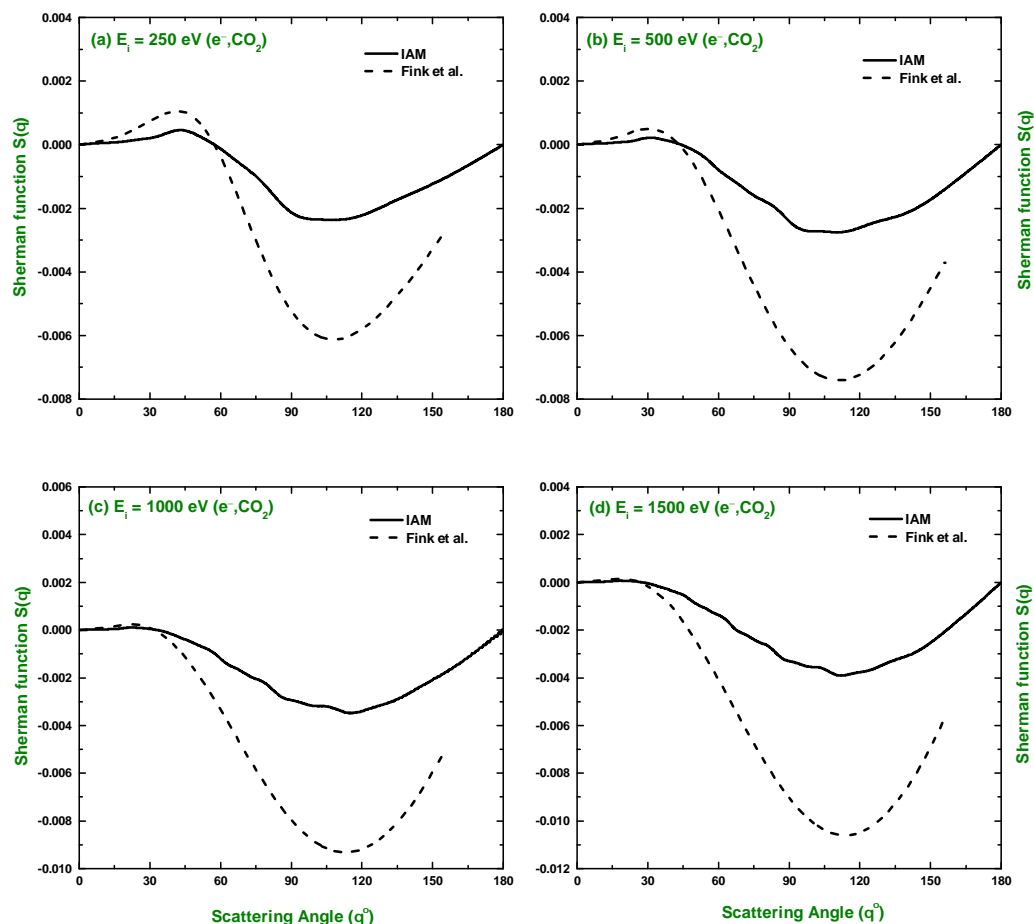
Figure 14. Angular dependence of the spin polarization of scattered electrons. References: available in Figure 13.

3.3. Total Cross-Section

In Figure 16a, we present our prediction of the total (elastic + inelastic) cross-section (TCS) for electron scattering from CO_2 molecules at 1 eV $\leq E_i \leq 1$ MeV. Our results are compared with the experimental data of Tanaka et al. [46], Iga et al. [52], Kwan et al. [57], Szmytkowski et al. [58], Nogueira et al. [59], Garcia and Manero [60], Hoffman et al. [61], and Shilin et al. [62]. The calculations of Iga et al. [45], Jain and Baluja [63] and the recommended data of Itikawa [14] are also included for comparison. As in Figure 16a, the calculations from the IAM and Jain and Baluja [63] overestimate all of the experimental results. In contrast, our IAMS, along with the calculations of Iga et al. [45], produce a good agreement with the experimental TCS of [47,48,57–61] at $E_i \geq 20$ eV. This observation is also true in the case of IECS, which is presented in Figure 16c.

Our IAMS calculation of the total ionization cross-section (TICS) for electron scattering is presented for $E_i = 10$–$10{,}000$ eV in Figure 16b. Additionally included are the predictions of Vinodkumar et al. [21] and Hwang et al. [64]. These three calculations are compared with the data measured by Asundi et al. [65], Craggs and Tozer [66], Rapp and Golden [67],

Orient and Srivastava [68], Freund et al.[69], Hudson et al. [20], and Straub et al. [70]. The comparison shows that our results and the other two calculations [21,64] agree well with the results of most of the experiments [20,67,68,70]. Our calculations underestimate the data of [65,66], but overestimate those of [69]. We think that more datasets (either theoretical or experimental) are needed to establish a reference set of TICS data for electron scattering by CO_2 molecules.
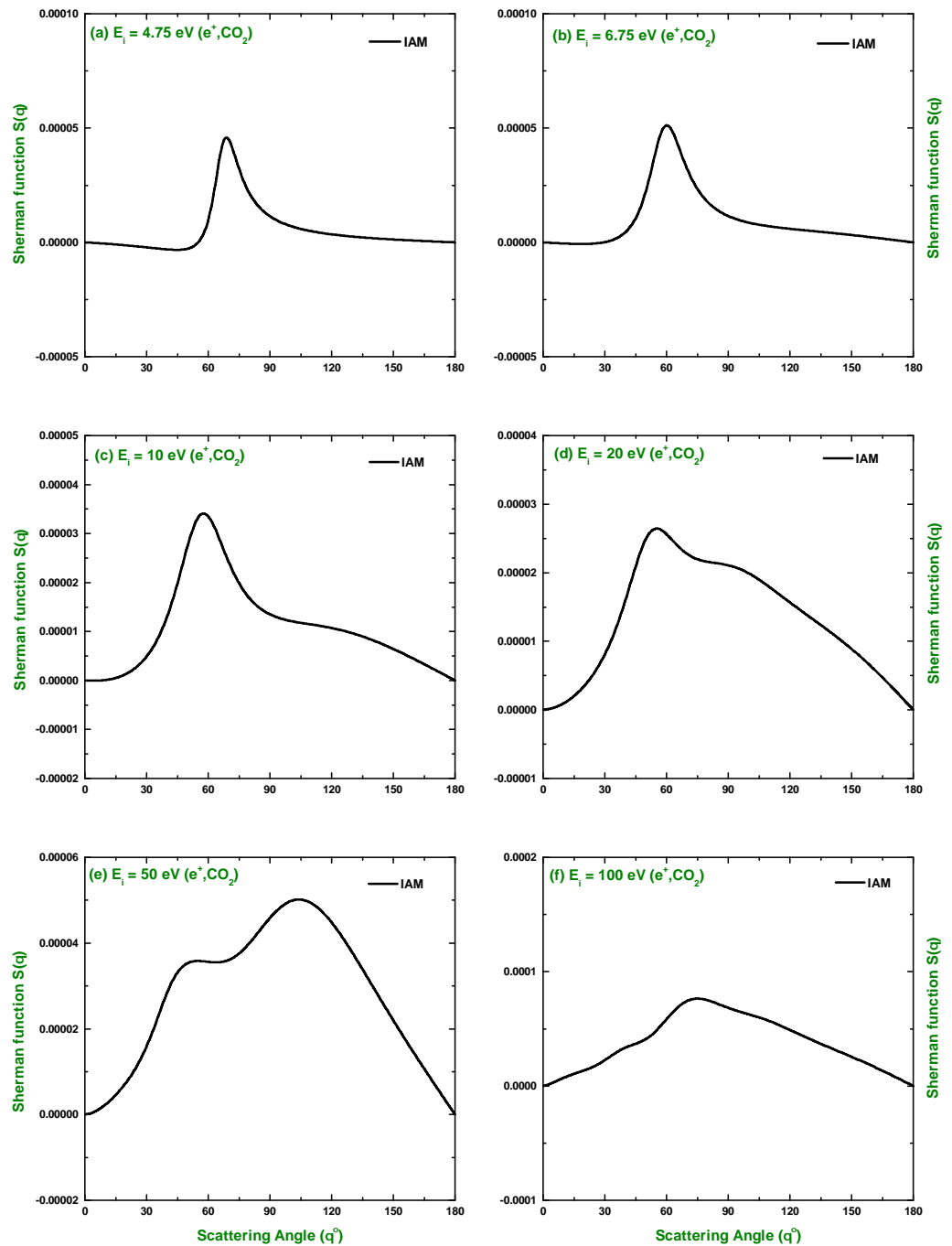
Figure 15. Angular dependence of the spin polarization of scattered positrons.
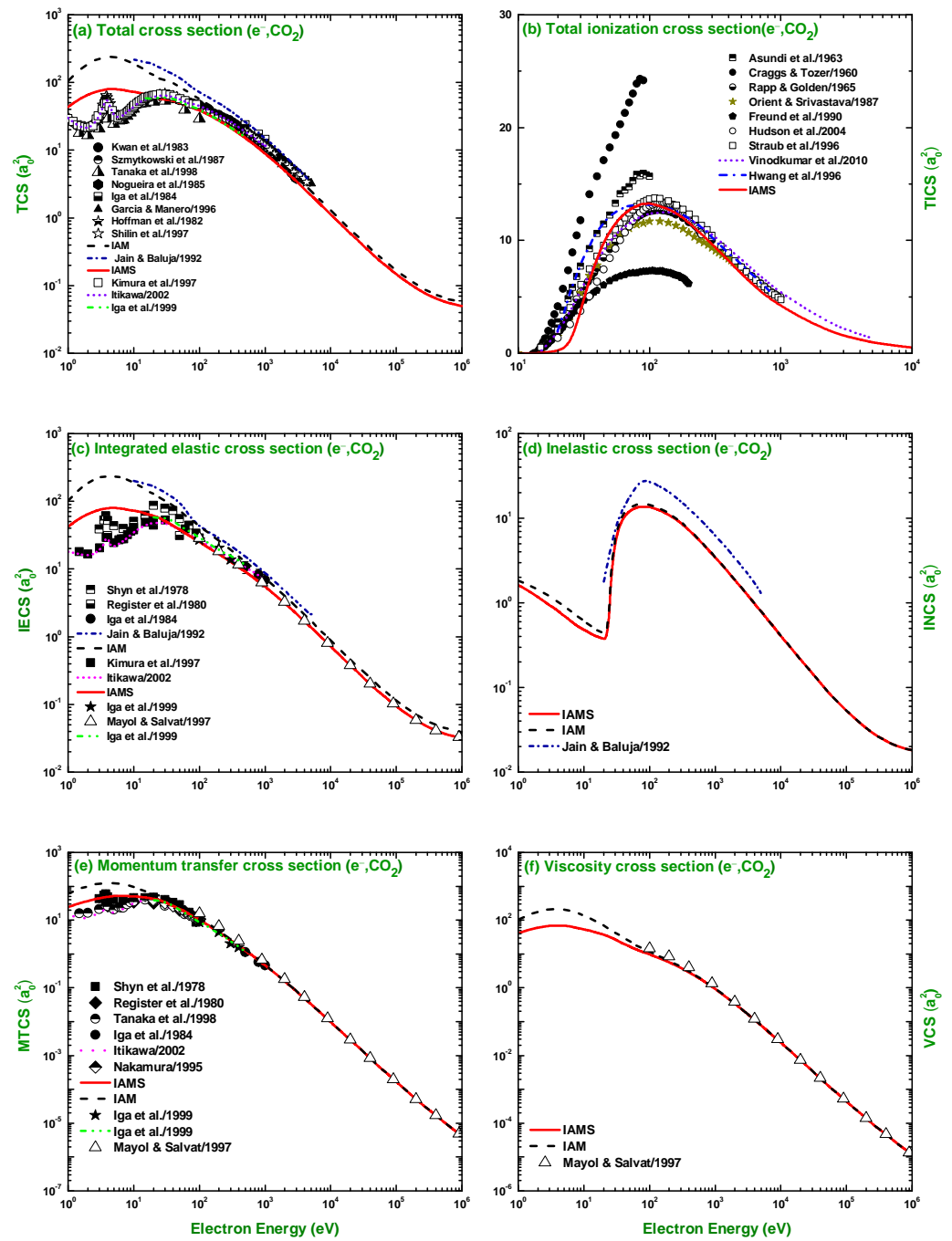
Figure 16. Values (a_0^2) of TCS, TICS, IECS, INCS, MTCS, and VCS for the scattering of electrons from carbon dioxide. Theoretical: IAM, IAMS, Vinodkumar et al. [21], Iga et al. [45], Jain and Baluja [63], Hwang et al. [64], and Mayol and Salvat [71]. Recommended: Itikawa [14]. Experimental: Hudson et al. [20], Iga et al. [45], Tanaka et al. [46], Shyn et al. [47], Register et al. [48], Iga et al. [52], Kwan et al. [57], Szmytkowski et al. [58], Nogueira et al. [59], Garcia and Manero [60], Hoffman et al. [61], Shilin et al. [62], Asundi et al. [65], Craggs and Tozer [66], Rapp and Golden [67], Orient and Srivastava [68], Freund et al. [69], Straub et al. [70], Kimura et al. [72] and Nakamura [73].

The present results of the IECS and MTCS are displayed, respectively, in Figure 16c,e, along with the experimental measurements [45–48,52,72,73]. Additionally included are the calculations of Iga et al. [45], Jain and Baluja [63], and Mayol and Salvat [71], as well as the recommended data of [14]. The theoretical data of [71] were generated by applying AR on their atomic data. As with the TCS and IECS, our IAMS result of MTCS produces

good agreement with the data and the calculations at $E_i \geq 20$ eV. Figures 16d,f show, respectively, the inelastic cross-section (INCS) and viscosity cross-section (VCS) due to both of our approaches (IAM and IAMS). No experimental measurements for these two observables are available in the literature. Therefore, we include the calculations of Jain and Baluja [63] and Mayol and Salvat [71] to compare with our results for the INCS and VCS, respectively. As is evident in Figure 16d, the INCS calculation of [63] shows disagreement with our results. As expected and explained earlier, a good agreement of the calculated results for IECS, MTCS, and VCS with those of [71] is observed throughout the compared energy range.

Table 1 presents the numerical values of the IECS, MTCS, VCS, INCS, TICS, and TCS for $e^- - CO_2$ scattering. It is worth mentioning that, at $E_i < 10$ eV, the TCS, IECS, and MTCS predicted by both of our methods (IAM and IAMS) and other approaches differ notably from the experimental results. In addition to that, no theoretical calculations are able to produce the shape resonance at $\sim$4 eV, except for the broader resonance at $\sim$30 eV. Theoretical approaches, such as R-matrix or multichannel calculations, might be able to reproduce these special low-energy features.

The TCS, TICS, IECS, INCS, MTCS, and VCS for positron scattering are displayed in Figure 17. The numerical results of these cross-sections for positron impact scattering are provided in Table 2. Our TCS results in Figure 17a are compared with the measured data from Kwan et al. [57], Hoffman et al. [61], Sueoka and Hamada [23], Charlton et al. [74,75], Zecca et al. [76], and Kimura et al. [72]. Additionally included in the comparison are theoretical calculations of Singh et al. [3] and Baluja and Jain [27]. The comparison shows a good agreement between our findings and the experiments at $E_i \geq 40$ eV. However, at lower energy (<40 eV), our results differ in magnitude but follow the pattern of the experimental data. This difference decreases with increasing energy. It is worth mentioning that a unique feature of positron impact scattering is the formation of Ps, the threshold of which for our current target CO_2 is 7 eV [53]. As in Figure 17a, the TCS suddenly increases from around 7 eV, which indicates Ps formation.

Figure 17b depicts our findings of the TICS for positron scattering in comparison with the experiments of Cooke et al. [26], Laricchia and Moxom [22], and Bluhme et al. [24], as well as the calculations of Singh and Antony [77] and Campeanu et al. [28]. As is evident in this figure, there are large discrepancies in the experimental data. However, we observe a reasonable agreement of our results with those of [77] and the data of [24]. The measured values from [22] are noticeably lower than those from the other experiments, our IAMS results, and other calculations [28,77].

Our IECS, INCS, MTCS, and VCS results for positron scattering are presented, respectively, in Figures 17c–f. We did not find any experimental data for these scattering observables in the literature to compare with our results. A significant variance is observed between our calculated INCSs and those of Singh et al. [3], as seen in Figure 17d, throughout the compared energy range.
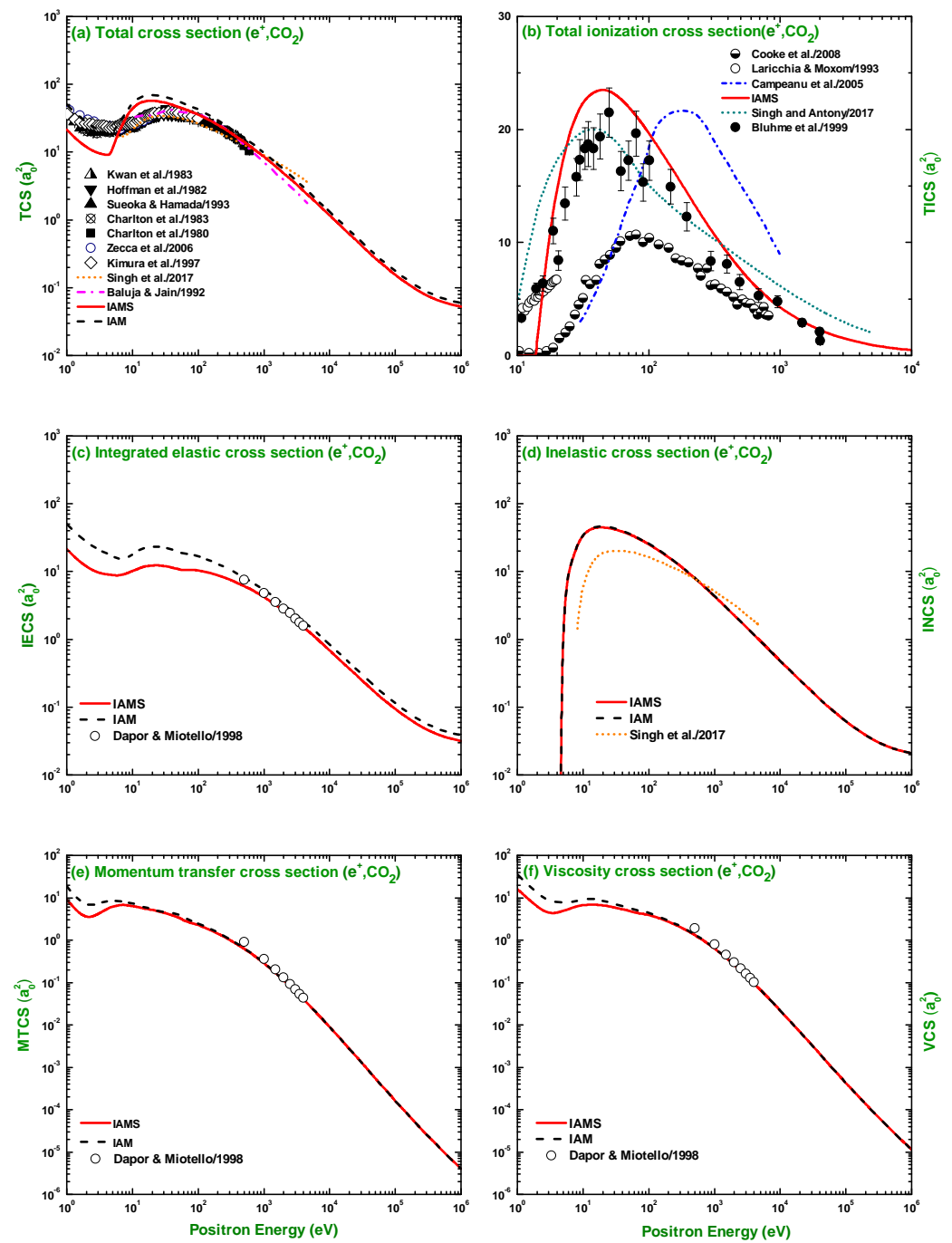
Figure 17. Values (a_0^2) of TCS, TICS, IECS, INCS, MTCS, and VCS for the scattering of positrons from carbon dioxide. Theoretical: IAM, IAMS, Singh et al. [3], Baluja and Jain [27], Campeanu et al. [28], Dapor and Miotello [54] and Singh and Antony [77]. Experimental: Laricchia and Moxom [22], Sueoka and Hamada [23], Bluhme et al. [24], Cooke et al. [26], Kwan et al. [57], Hoffman et al. [61], Kimura et al. [72], Charlton et al. [74,75], and Zecca et al. [76].

Table 1. Elastic total (IECS), momentum-transfer (MTCS), viscosity (VCS), inelastic (INCS), and total (TCS) cross-sections for electron scattering from CO_2.

Energy (eV)	IECS (a_0^2)	MTCS (a_0^2)	VCS (a_0^2)	INCS (a_0^2)	TCS (a_0^2)	Energy (eV)	IECS (a_0^2)	MTCS (a_0^2)	VCS (a_0^2)	INCS (a_0^2)	TCS (a_0^2)
1.0	42.0854	23.98482	41.07042	1.638150	43.72359	500	9.08970	1.26628	2.24338	6.10128	15.19098
1.5	56.1819	31.55945	53.25334	1.362240	57.54414	550	8.50429	1.10932	2.00673	5.66504	14.16933
2.0	64.8906	36.91512	60.25945	1.171040	66.06168	600	7.99641	0.98165	1.80794	5.28682	13.28323
2.5	70.4222	40.94651	64.35240	1.033250	71.45554	650	7.55041	0.87605	1.63892	4.95605	12.50646
3.0	74.6747	44.46517	67.35923	0.940170	75.61496	700	7.15491	0.78753	1.49379	4.66444	11.81935
3.5	77.3191	47.07412	68.85656	0.864100	78.18324	750	6.80126	0.71246	1.36808	4.40550	11.20676
4.0	78.8274	48.96623	69.28283	0.800820	79.62824	800	6.48279	0.64815	1.25836	4.17406	10.65685
4.5	79.5257	50.28929	68.94716	0.748320	80.27407	850	6.19423	0.59258	1.16195	3.96597	10.16021
5.0	79.6438	51.15950	68.07291	0.703410	80.34728	900	5.93137	0.54418	1.07672	3.77789	9.70926
6.0	78.7427	51.88624	65.31629	0.630560	79.37326	950	5.69081	0.50173	1.00096	3.60704	9.29784
7.0	76.9509	51.67313	61.86663	0.574800	77.52578	1000	5.46970	0.46427	0.93328	3.45116	8.92086
8.0	75.0720	51.09960	58.51929	0.533000	75.60503	1500	3.95256	0.24702	0.52331	2.41427	6.36683
9.0	73.8490	50.73996	55.95032	0.503300	74.35231	2000	3.10288	0.15521	0.33902	1.86027	4.96315
10	72.6002	50.21334	53.53634	0.479610	73.07981	2500	2.55727	0.10736	0.23939	1.51489	4.07215
11	71.3549	49.58229	51.29557	0.459590	71.81454	3000	2.17672	0.07909	0.17906	1.27863	3.45536
12	70.1252	48.88473	49.22426	0.443350	70.56856	3500	1.89591	0.06092	0.13955	1.10677	3.00268
13	68.9171	48.14579	47.30963	0.429340	69.34652	4000	1.68007	0.04851	0.11217	0.97607	2.65614
14	67.7322	47.38034	45.53585	0.417790	68.15004	4500	1.50898	0.03963	0.09236	0.87329	2.38227
15	66.5713	46.59925	43.88764	0.407600	66.97898	5000	1.36997	0.03305	0.07753	0.79035	2.16032
16	65.4344	45.80875	42.35064	0.399210	65.83361	5500	1.25478	0.02802	0.06611	0.72200	1.97678
17	64.3217	45.01423	40.91303	0.391780	64.71351	6000	1.15775	0.02409	0.05712	0.66470	1.82245
18	63.2330	44.21868	39.56436	0.385840	63.61887	6500	1.07489	0.02096	0.04991	0.61598	1.69087
19	62.1688	43.42543	38.29632	0.380690	62.54957	7000	1.00331	0.01841	0.04402	0.57404	1.57735
20	61.1293	42.63653	37.10176	0.376440	61.50576	7500	0.94084	0.01632	0.03915	0.53756	1.47840
22	59.1249	41.07920	34.91004	0.370410	59.49532	8000	0.88585	0.01457	0.03508	0.50553	1.39138
24	57.1988	39.51914	32.90082	0.633270	57.83212	8500	0.83707	0.01310	0.03163	0.47719	1.31426
25	56.2152	38.65356	31.88650	1.068660	57.28394	9000	0.79351	0.01184	0.02868	0.45193	1.24544
26	55.1807	37.66610	30.83114	1.783060	56.96381	9500	0.75436	0.01077	0.02614	0.42928	1.18364
28	53.1045	35.59678	28.77283	3.450760	56.55532	10,000	0.71899	0.00984	0.02393	0.40885	1.12784
30	51.1376	33.62184	26.90229	5.019120	56.15674	15,000	0.48923	0.00479	0.01186	0.27850	0.76773
32	49.3114	31.80384	25.23542	6.387610	55.69908	20,000	0.37474	0.00287	0.00718	0.21268	0.58742
35	46.8329	29.37655	23.08099	8.073230	54.90616	25,000	0.30529	0.00193	0.00486	0.17297	0.47826
40	43.3393	26.06374	20.25115	10.03933	53.37863	30,000	0.25867	0.00139	0.00353	0.14640	0.40508
45	40.4751	23.42668	18.12230	11.31222	51.78741	40,000	0.20005	8.32×10^{-4}	0.00214	0.11310	0.31315
50	38.0845	21.26576	16.48502	12.15395	50.23855	50,000	0.16471	5.60×10^{-4}	0.00145	0.09306	0.25777
55	35.9628	19.46319	15.21109	12.72534	48.68822	60,000	0.14108	4.06×10^{-4}	0.00106	0.07968	0.22076
60	34.1392	17.90347	14.18016	13.11308	47.25237	70,000	0.12418	3.09×10^{-4}	8.09×10^{-4}	0.07013	0.19430
65	32.5491	16.53843	13.32758	13.37236	45.92153	80,000	0.11149	2.45×10^{-4}	6.43×10^{-4}	0.06296	0.17445
70	31.1420	15.33249	12.60837	13.53775	44.67976	90,000	0.10162	1.99×10^{-4}	5.26×10^{-4}	0.05738	0.15901
75	29.8818	14.25735	11.98851	13.63682	43.51870	100,000	0.09373	1.66×10^{-4}	4.404×10^{-4}	0.05293	0.14666
80	28.7444	13.29421	11.44535	13.68409	42.42852	150,000	0.07011	8.32×10^{-5}	2.23×10^{-4}	0.03960	0.10971
85	27.7103	12.42691	10.96134	13.69332	41.40366	200,000	0.05839	5.15×10^{-5}	1.39×10^{-4}	0.03299	0.09138
90	26.7664	11.64579	10.52648	13.66786	40.43429	250,000	0.05143	3.57×10^{-5}	9.74×10^{-5}	0.02906	0.08049
95	25.9004	10.93954	10.13083	13.61692	39.51739	300,000	0.04684	2.67×10^{-5}	7.30×10^{-5}	0.02648	0.07332
100	25.1031	10.29893	9.767290	13.54679	38.64990	400,000	0.04122	1.69×10^{-5}	4.67×10^{-5}	0.02331	0.06453
150	19.5995	6.25218	7.21430	12.31879	31.91836	500,000	0.03795	1.20×10^{-5}	3.32×10^{-5}	0.02146	0.05941
200	16.4716	4.33727	5.70653	10.90102	27.37261	600,000	0.03583	9.04×10^{-6}	2.52×10^{-5}	0.02028	0.05611
250	14.3514	3.23499	4.66128	9.70991	24.06132	700,000	0.03437	7.14×10^{-6}	2.00×10^{-5}	0.01945	0.05382
300	12.7780	2.52920	3.89092	8.73757	21.51563	800,000	0.03331	5.83×10^{-6}	1.64×10^{-5}	0.01884	0.05214
350	11.5650	2.05474	3.31937	7.90969	19.47475	900,000	0.03251	4.87×10^{-6}	1.37×10^{-5}	0.01842	0.05093
400	10.5895	1.71708	2.88076	7.20521	17.79471	1,000,000	0.03189	4.15×10^{-6}	1.17×10^{-5}	0.01808	0.04997
450	9.77496	1.46330	2.52934	6.60900	16.38396	-	-	-	-	-	-

Table 2. Elastic total (IECS), momentum-transfer (MTCS), viscosity (VCS), inelastic (INCS), and total (TCS) cross-sections for positron scattering from CO_2.

Energy (eV)	IECS (a_0^2)	MTCS (a_0^2)	VCS (a_0^2)	INCS (a_0^2)	TCS (a_0^2)	Energy (eV)	IECS (a_0^2)	MTCS (a_0^2)	VCS (a_0^2)	INCS (a_0^2)	TCS (a_0^2)
1.0	21.31376	9.04547	16.16806	—	21.31376	500	6.13463	0.62842	1.32568	7.988410	14.12304
1.5	14.64154	4.41747	9.09951	—	14.64154	550	5.86076	0.56935	1.21088	7.360950	13.22171
2.0	11.77617	3.41346	6.18675	—	11.77617	600	5.61262	0.51897	1.11161	6.825040	12.43766
2.5	10.39729	3.58501	4.94863	—	10.39729	650	5.38628	0.47554	1.02498	6.362100	11.74838
3.0	9.683410	4.12826	4.47923	—	9.683410	700	5.17866	0.43773	0.94881	5.958260	11.13692
3.5	9.294760	4.74907	4.38943	—	9.294760	750	4.98736	0.40458	0.88137	5.602900	10.59026
4.0	9.075470	5.33761	4.49373	—	9.075470	800	4.81038	0.37530	0.82132	5.28781	10.09819
4.5	8.947990	5.85614	4.69675	0.022530	8.970520	850	4.64608	0.34928	0.76759	5.00652	9.65260
5.0	8.791060	6.21986	4.90586	2.493160	11.28422	900	4.49309	0.32604	0.71928	4.75386	9.24696
6.0	8.706730	6.60407	5.38391	10.02620	18.73293	950	4.35028	0.30520	0.67567	4.52567	8.87595
7.0	8.995430	6.81869	5.90467	15.58556	24.58100	1000	4.21664	0.28641	0.63616	4.31851	8.53515
8.0	9.335050	6.76016	6.26459	22.48894	31.82399	1500	3.23440	0.16869	0.38346	2.96623	6.20063
9.0	9.722720	6.55397	6.49990	28.99780	38.72052	2000	2.63111	0.11290	0.26023	2.26187	4.89298
10	10.15614	6.33429	6.66653	34.09654	44.25268	2500	2.22138	0.08161	0.18997	1.82930	4.05068
11	10.57529	6.14749	6.78050	37.68302	48.25831	3000	1.92427	0.06213	0.14571	1.53650	3.46077
12	10.95133	5.99034	6.84942	40.18165	51.13298	3500	1.69864	0.04909	0.11583	1.32509	3.02373
13	11.27257	5.85506	6.88140	41.90944	53.18201	4000	1.52132	0.03989	0.09461	1.16524	2.68656
14	11.53878	5.73596	6.88474	43.09077	54.62955	4500	1.37819	0.03313	0.07894	1.04014	2.41833
15	11.75516	5.62711	6.86672	43.87846	55.63362	5000	1.26018	0.02801	0.06700	0.93956	2.19974
16	11.92770	5.52692	6.83287	44.38120	56.30889	5500	1.16118	0.02403	0.05768	0.85694	2.01812
17	12.06341	5.43239	6.78744	44.67995	56.74336	6000	1.07691	0.02086	0.05025	0.78785	1.86477
18	12.16665	5.34237	6.73368	44.82097	56.98762	6500	1.00431	0.01830	0.04422	0.72923	1.73354
19	12.24139	5.25615	6.67412	44.83814	57.07953	7000	0.94109	0.01620	0.03925	0.67887	1.61996
20	12.29155	5.17318	6.61067	44.75847	57.05002	7500	0.88555	0.01446	0.03510	0.63513	1.52068
22	12.34065	5.01289	6.47673	44.43228	56.77294	8000	0.83635	0.01299	0.03161	0.59679	1.43314
24	12.32951	4.86104	6.33969	43.92987	56.25939	8500	0.79248	0.01173	0.02863	0.56291	1.35538
25	12.30806	4.78775	6.27134	43.63920	55.94726	9000	0.75310	0.01066	0.02606	0.53275	1.28584
26	12.27922	4.71585	6.20348	43.33667	55.61589	9500	0.71755	0.00973	0.02384	0.50573	1.22328
28	12.19977	4.57739	6.07058	42.68939	54.88916	10,000	0.68531	0.00893	0.02190	0.48139	1.16670
30	12.10260	4.44497	5.94177	42.02174	54.12434	15,000	0.47788	0.00446	0.01110	0.32664	0.80452
32	11.98864	4.31973	5.81869	41.33653	53.32517	20,000	0.36790	0.00271	0.00680	0.24891	0.61680
35	11.80039	4.14345	5.64396	40.30803	52.10842	25,000	0.30065	0.00183	0.00464	0.20214	0.50279
40	11.47062	3.87874	5.37857	38.65748	50.12810	30,000	0.25528	0.00133	0.00338	0.17093	0.42621
45	11.13984	3.64701	5.14290	37.10724	48.24707	40,000	0.19796	8.00×10^{-4}	0.00206	0.13186	0.32982
50	10.82024	3.44391	4.93337	35.66469	46.48493	50,000	0.16325	5.40×10^{-4}	0.00140	0.10841	0.27166
55	10.59385	3.16367	4.69440	34.21506	44.80891	60,000	0.13998	3.92×10^{-4}	0.00102	0.09277	0.23276
60	10.55688	2.97217	4.55067	32.89154	43.44841	70,000	0.12331	2.99×10^{-4}	7.84×10^{-4}	0.08161	0.20492
65	10.55709	2.82815	4.44206	31.67675	42.23384	80,000	0.11078	2.37×10^{-4}	6.24×10^{-4}	0.07324	0.18402
70	10.56426	2.71101	4.34963	30.55911	41.12338	90,000	0.10103	1.93×10^{-4}	5.10×10^{-4}	0.06673	0.16776
75	10.56748	2.61247	4.26708	29.52444	40.09192	100,000	0.09322	1.61×10^{-4}	4.27×10^{-4}	0.06153	0.15475
80	10.56155	2.52664	4.18951	28.56732	39.12887	150,000	0.06981	8.06×10^{-5}	2.17×10^{-4}	0.04600	0.11581
85	10.54226	2.45203	4.11741	27.66548	38.20774	200,000	0.05818	4.98×10^{-5}	1.35×10^{-4}	0.03830	0.09648
90	10.51084	2.38396	4.04624	26.82760	37.33844	250,000	0.05127	3.46×10^{-5}	9.45×10^{-5}	0.03373	0.08500
95	10.46829	2.32201	3.97679	26.04335	36.51163	300,000	0.04671	2.58×10^{-5}	7.09×10^{-5}	0.03073	0.07744
100	10.41215	2.26253	3.90614	25.30739	35.71954	400,000	0.04112	1.64×10^{-5}	4.53×10^{-5}	0.02704	0.06816
150	9.58138	1.76368	3.23099	19.81904	29.40042	500,000	0.03787	1.16×10^{-5}	3.22×10^{-5}	0.02488	0.06275
200	8.80091	1.42913	2.72322	16.33623	25.13714	600,000	0.03577	8.73×10^{-6}	2.45×10^{-5}	0.02351	0.05928
250	8.16199	1.19573	2.34308	13.90700	22.06899	700,000	0.03431	6.90×10^{-6}	1.94×10^{-5}	0.02254	0.05685
300	7.62864	1.02244	2.04751	12.11221	19.74085	800,000	0.03326	5.63×10^{-6}	1.59×10^{-5}	0.02182	0.05508
350	7.17515	0.88922	1.81158	10.72907	17.90422	900,000	0.03246	4.71×10^{-6}	1.33×10^{-5}	0.02136	0.05382
400	6.78321	0.78391	1.61935	9.628990	16.41220	1,000,000	0.03184	4.01×10^{-6}	1.13×10^{-5}	0.02096	0.05280
450	6.43951	0.69868	1.45990	8.732760	15.17227	-	-	-	-	-	-

4. Conclusions

This paper reports on the elastic differential cross-section, total (elastic + inelastic) cross-section, integrated elastic cross-section, inelastic cross-section, momentum-transfer cross-section, viscosity cross-section, total ionization cross-section, and spin polarization for both the electron and positron impact scattering from CO_2 molecules over a wide range of incident energy of $1 \text{ eV} \leq E_i \leq 1 \text{ MeV}$ and scattering angles of $0° \leq \theta \leq 180°$. All of the above scattering observables were calculated within the framework of Dirac partial-wave analysis. The procedure of calculation adopted the IAM and IAMS approaches, as explained earlier, which employ projectile–atom interaction instead of projectile–molecule interaction. Our study revealed that the inclusion of the screening effect improved the quality of our predictions by reducing the cross-sections at low energies and angles.

For positron projectiles, the scattering observables show some different features. The cross-section produces less of a structure and is smaller in magnitude. However, the additional consideration of the correlation-polarization potential produces some structures in the positron impact cross-section and in the spin asymmetry, but only up to $E_i \sim 100$ eV. As a consequence of the dominance of the nuclear Coulomb field, both the cross-section and Sherman function are reduced by several orders of magnitude as compared to their electron counterparts.

Our findings were compared with the available experimental results and other theoretical results that were obtained by using different methods and potentials. It is worth mentioning that, for the first time, we have reported on several collision cross-sections over such a wide range of energies. The comparison shows that our screening-corrected results reasonably agree with the available experimental measurements and other theoretical findings. However, the present predictions at energies of <20 eV show conspicuous discrepancies with the experimental data in and around the minimum region. It is well known that, before the onset of the inelastic threshold, the optical potential is not suitable for accurately modeling the invasion of a substantial contribution of the resonance elastic channel corresponding to the isolated levels of a composite system. Despite this limitation, the present study reveals that our screen-corrected theory (IAMS) is capable of generating cross-sections reasonably well, apart from those at very low energies. This simple method might be used to produce useful data for other molecules, which are immensely needed in the modeling of material and biological processes. More data are needed for further refinement of the theory. Our predictions for positrons still await verification by future experiments.

Author Contributions: M.M.B.: investigation, formal analysis, and writing—review and editing; M.M.K.: investigation; M.M.H.: writing—original draft preparation and editing; M.Y.A.: data curation; M.H.K.: visualization; A.K.F.H.: methodology and supervision; H.W.: review and resources; M.A.U.: conceptualization, software, review, and validation. All authors have read and agreed to the submitted version of the manuscript.

Conflicts of Interest: The authors declare no conflict of interest.

References

1. Watanabe, T.; Shimamura, I.; Shimizu, M.; Itakawa, Y. (Eds.) *Molecular Processes in Space*; Plenum: New York, NY, USA, 1990.
2. Liu, W.; Victor, G.A. Electron energy deposition in carbon monoxide gas. *Astro Phys. J.* **1994**, *435*, 909. [CrossRef]
3. Singh, S.; Dutta, S.; Naghma, R.; Antony, B. Positron scattering from simple molecules. *J. Phys. B At. Mol. Opt. Phys.* **2017**, *50*, 135202. [CrossRef]
4. Christophorou, L.G. (Ed.) *Electron Molecule Interactions and Their Applications*; Academic: New York, NY, USA, 1984; Volumes 1 and 2.
5. Jain, A.; Freitas, L.C.G.; Mu-Tao, L.; Tayal, S.S. Elastic scattering of intermediate and high energy electrons with N_2 and CO molecules. *J. Phys. B At. Mol. Phys.* **1984**, *17*, L29. [CrossRef]
6. Hassan, R.; Abdullah, M.N.; Shorifuddoza, M.; Khandker, M.H.; Patoary, M.A.; Haque, M.M.; Das, P.K.; Maaza, M.; Billah, M.M.; Haque, A.K.; et al. Scattering of $e^{\pm}$ off silver atom over the energy range 1 eV–1 MeV. *Eur. Phys. J. D* **2021**, *75*, 1–23. [CrossRef]

7. Afroz, S.; Haque, M.M.; Haque, A.F.; Jakubassa-Amundsen, D.H.; Patoary, M.A.; Shorifuddoza, M.; Khandker, M.H.; Uddin, M.A. Elastic scattering of electrons and positrons from ^{115}In atoms over the energy range 1 eV–0.5 GeV. *Results Phys.* **2020**, *18*, 103179. [CrossRef]

8. Hassan, R.; Haque, M.M.; Haque, A.K.; Shorifuddoza, M.; Khandker, M.H.; Patoary, M.A.; Basak, A.K.; Maaza, M.; Saha, B.C.; Uddin, M.A. Relativistic study on the scattering of electrons and positrons from atomic iron at energies 1 eV–10 keV. *Mol. Phys.* **2020**, *23*, e1849838. [CrossRef]

9. Haque, M.M.; Haque, A.K.; Jakubassa-Amundsen, D.H.; Patoary, M.A.; Basak, A.K.; Maaza, M.; Saha, B.C.; Uddin, M.A. e$^{\pm}$-Ar scattering in the energy range 1 eV$\leq E_i \leq$ 0.5 GeV. *J. Phys. Commun.* **2019**, *3*, 045011. [CrossRef]

10. Haque, M.M.; Haque, A.K.; Bhattacharjee, P.P.; Uddin, M.A.; Patoary, M.A.; Basak, A.K.; Maaza, M.; Saha, B.C. Relativistic treatment of scattering of electrons and positrons by mercury atoms. *Mol. Phys.* **2019**, *117*, 2303–2319. [CrossRef]

11. Haque, A.K.; Haque, M.M.; Hossain, M.S.; Hossain, M.I.; Patoary, M.A.; Maaza, M.; Basak, A.K.; Saha, B.C.; Uddin, M.A. A study of the critical minima and spin polarization in the elastic electron scattering by the lead atom. *J. Phys. Commun.* **2018**, *2*, 125013. [CrossRef]

12. Hosain, M.E.; Patoary, M.A.; Haque, M.M.; Haque, A.F.; Hossain, M.I.; Uddin, M.A.; Basak, A.K.; Maaza, M.; Saha, B.C. Elastic scattering of e$^{\pm}$ by Na atoms. *Mol. Phys.* **2018**, *116*, 631–648. [CrossRef]

13. McWilliam, A.; Rauch, M. (Eds.) *Origin and Evolution of the Elements (Carnegie Observatories Astrophysics Series Volume 4)*; Cambridge University Press: Cambridge, UK, 2014.

14. Itikawa, Y. Cross sections for electron collisions with carbon dioxide. *J. Phys. Chem. Ref. Data* **2002**, *31*, 749. [CrossRef]

15. Jackman, C.H.; Garvey, R.H.; Green, A.E. Electron impact on atmospheric gases, I. Updated cross sections. *J. Geophys. Res.* **1977**, *82*, 5081–5090. [CrossRef]

16. Itikawa, Y.; Shimizu, M. Effective cross sections for collision processes between carbon dioxide and slow electrons, with application to the Martian upper atmosphere. *Bull. Inst. Space Aeronaut. Sci.* **1971**, *7*, 64.

17. Tawara, H. *Atomic and Molecular Data for H$_2$O, CO and CO$_2$ Relevant to Edge Plasma Impurities*; NIFS Report NIFS-DATA-19; National Institute for Fusion Science: Toki, Japan, 1992.

18. Shirai, T.; Tabata, T.; Tawara, H. Analytic cross sections for electron collisions with CO, CO$_2$, and H$_2$O relevant to edge plasma impurities. *At. Data Nucl. Data Tables* **2001**, *79*, 143–184. [CrossRef]

19. Karwasz, G.P.; Brusa, R.S.; Zecca, A. One century of experiments on electron-atom and molecule scattering: A critical review of integral cross-sections. *Riv. Nuovo C.* **2001**, *24*, 1–118. [CrossRef]

20. Hudson, J.E.; Vallance, C.; Harl, P.W. Absolute electron impact ionization cross-sections for CO, CO$_2$, OCS and CS$_2$. *J. Phys. B At. Mol. Opt. Phys.* **2003**, *37*, 445. [CrossRef]

21. Vinodkumar, M.; Limbachiya, C.; Bhutadia, H. Electron impact calculations of total ionization cross sections for environmentally sensitive diatomic and triatomic molecules from threshold to 5 keV. *J. Phys. B At. Mol. Opt. Phys.* **2009**, *43*, 015203. [CrossRef]

22. Laricchia, G.; Moxom, J. Ionization of CO$_2$ by positron impact. *Phys. Lett. A* **1993**, *174*, 255–257. [CrossRef]

23. Sueoka, O.; Hamada, A. Total cross-section measurements for 0.3–10 eV positron scattering on N2, CO, and CO$_2$ molecules. *J. Phys. Soc. Jpn.* **1993**, *62*, 2669–2674. [CrossRef]

24. Bluhme, H.; Frandsen, N.P.; Jacobsen, F.M.; Knudsen, H.; Merrison, J.P.; Mitchell, R.; Paludan, K.; Poulsen, M.R. Non-dissociative and dissociative ionization of CO, CO$_2$ and CH$_4$ by positron impact. *J. Phys. B At. Mol. Opt. Phys.* **1999**, *32*, 5825. [CrossRef]

25. Marler, J.P.; Surko, C.M. Positron-impact ionization, positronium formation, and electronic excitation cross sections for diatomic molecules. *Phys. Rev. A* **2005**, *72*, 062713 [CrossRef]

26. Cooke, D.A.; Murtagh, D.J.; Kövér, A.; Laricchia, G. Direct non-dissociative and dissociative ionization of CO$_2$ by positron impact. *Nucl. Instrum. Methods Phys. Res. Sect. Beam Interact. Mater. Atoms.* **2008**, *266*, 466–470. [CrossRef]

27. Baluja, K.L.; Jain, A. Total (elastic and inelastic) scattering cross sections for several positron-molecule systems at 10–5000 eV: H$_2$, H$_2$O, NH$_3$, CH$_4$, N$_2$, CO, C$_2$H$_2$, O$_2$, SiH4, CO$_2$, N$_2$O, and CF$_4$. *Phys. Rev. A* **1992**, *45*, 7838. [CrossRef]

28. Campeanu, R.I.; Chis, V.; Nagy, L.; Stauffer, A.D. Positron impact ionization of CO and CO$_2$. *Phys. Lett. A* **2005**, *344*, 247–252. [CrossRef]

29. Blanco, F.; Garcia, G. Screening corrections for calculation of electron scattering from polyatomic molecules. *Phys. Lett. A* **2003**, *317*, 458–462. [CrossRef]

30. Blanco, F.; Ellis-Gibbings, L.; García, G. Screening corrections for the interference contributions to the electron and positron scattering cross sections from polyatomic molecules. *Chem. Phys. Lett.* **2016**, *645*, 71–75. [CrossRef]

31. Billah, M.M.; Khandker, M.H.; Shorifuddoza, M.; Sayed, M.A.; Watabe, H.; Haque, A.K.; Uddin, M.A. Theoretical investigations of e$^{\pm}$–CO scattering. *J. Phys. B At. Mol. Opt. Phys.* **2021**, *54*, 095203. [CrossRef]

32. Dirac, P.A.M. *Relativistic Theory of the Electron, International Series of Monographs on Physics*, 4th ed.; Oxford University Press: New York, NY, USA, 1981.

33. Salvat, F.; Fernandez-Varea, J.M.; Williamson, W. Accurate numerical solution of the radial Schrödinger and Dirac wave equations. *Comput. Phys. Commun.* **1995**, *90*, 151–168. [CrossRef]

34. Salvat, F.; Jablonski, A.; Powell, C.J. ELSEPA—Dirac partial-wave calculation of elastic scattering of electrons and positrons by atoms, positive ions and molecules. *Comput. Phys. Commun.* **2005**, *165*, 157–190. [CrossRef]

35. Desclaux, J.P. A multiconfiguration relativistic Dirac-Fock program. *Comput. Phys. Commun.* **1975**, *9*, 31–45. [CrossRef]

36. Hahn, B.; Ravenhall, D.G.; Hofstadter, R. High-energy electron scattering and the charge distributions of selected nuclei. *Phys. Rev.* **1956**, *101*, 1131 [CrossRef]

37. Furness, J.B.; McCarthy, I.E. Semiphenomenological optical model for electron scattering on atoms. *Phys. At. B Mol. Phys.* **1973**, *6*, 2280. [CrossRef]

38. Salvat, F. Optical-model potential for electron and positron elastic scattering by atoms. *Phys. Rev. A* **2003**, *68*, 012708. [CrossRef]

39. Hossain, M.I.; Haque, A.K.; Atiqur, M.; Patoary, R.; Uddin, M.A.; Basak, A.K. Elastic scattering of electrons and positrons by atomic magnesium. *Eur. Phys. J. D* **2016**, *70*, 1–9.

40. Lide, D.R. (Ed.) *CRC Handbook of Chemistry and Physics (Volume 85)*; CRC Press: Boca Raton, FL, USA, 2004.

41. Available online: https://cccbdb.nist.gov/pollistx.asp (accessed on 21 August 2020).

42. Zhan, C.G.; Nichols, J.A.; Dixon, D.A. Ionization potential, electron affinity, electronegativity, hardness, and electron excitation energy: Molecular properties from density functional theory orbital energies. *J. Phys. Chem. A* **2003**, *107*, 4184–4195. [CrossRef]

43. Joshipura, K.N.; Antony, B.K. Total (including ionization) cross sections of electron impact on ground state and metastable Ne atoms. *Phys. Lett. A* **2001**, *289*, 323–328. [CrossRef]

44. Joshipura, K.N.; Limbachiya, C.G. 2002 Theoretical total ionization cross-sections for electron impact on atomic and molecular halogens. *Int. J. Mass Spectrom.* **2002**, *216*, 239–247 [CrossRef]

45. Iga, I.; Homem, M.G.; Mazon, K.T.; Lee, M.T. Elastic and total cross sections for electron-carbon dioxide collisions in the intermediate energy range. *J. Phys. At. Mol. Opt. Phys.* **1999**, *32*, 4373. [CrossRef]

46. Tanaka, H.; Ishikawa, T.; Masai, T.; Sagara, T.; Boesten, L.; Takekawa, M.; Itikawa, Y.; Kimura, M. Elastic collisions of low-to-intermediate-energy electrons from carbon dioxide: Experimental and theoretical differential cross sections. *Phys. Rev. A* **1998**, *57*, 1798. [CrossRef]

47. Shyn, T.W.; Sharp, W.E.; Carignan, G.R. Angular distribution of electrons elastically scattered from CO_2. *Phys. Rev. A* **1978**, *17*, 1855. [CrossRef]

48. Register, D.F.; Nishimura, H.; Trajmar, S. Elastic scattering and vibrational excitation of CO_2 by 4, 10, 20 and 50 eV electrons. *J. Phys. B At. Mol. Phys.* **1980**, *13*, 1651. [CrossRef]

49. Kanik, I.; McCollum, D.C.; Nickel, J.C. Absolute elastic differential scattering cross sections for electron impact on carbon dioxide in the intermediate energy region. *J. Phys. B At. Mol. Opt. Phys.* **1989**, *22*, 1225. [CrossRef]

50. Bromberg, J.P. Absolute differential cross sections of elastically scattered electrons. V. O_2 and CO_2 at 500, 400, and 300 eV. *J. Chem. Phys.* **1974**, *60*, 1717–1721. [CrossRef]

51. Maji, S.; Basavaraju, G.; Bharathi, S.M.; Bhushan, K.G.; Khare, S.P. Elastic scattering of electrons by polyatomic molecules in the energy range 300–1300 eV: CO, H and. *J. Phys. B At. Mol. Opt. Phys.* **1998**, *31*, 4975. [CrossRef]

52. Iga, I.; Nogueira, J.C.; Mu-Tao, L. Elastic scattering of electrons from CO_2 in the intermediate energy range. *J. Phys. B At. Mol. Phys.* **1984**, *17*, L185. [CrossRef]

53. Przybyla, D.A.; Addo-Asah, W.; Kauppila, W.E.; Kwan, C.K.; Stein, T.S. Measurements of differential cross sections for positrons scattered from N_2, CO, O_2, N_2O, and CO_2. *Phys. Rev. A* **1999**, *60*, 359. [CrossRef]

54. Dapor, M.; Miotello, A. Differential, total, and transport cross sections for elastic scattering of low energy positrons by neutral atoms (Z = 1–92, E = 500–4000 eV). *At. Data Nucl. Data Tables* **1998**, *69*, 1–100. [CrossRef]

55. Fink, M.; Yates, A.C. Theoretical electron scattering amplitudes and spin polarizations. *At. Data Nucl. Data Tables* **1969**, *1*, 385–456. [CrossRef]

56. Fink, M.; Ingram, J. Theoretical electron scattering amplitudes and spin polarizations: Electron energies 100 to 1500 eV Part II. Be, N, O, Al, Cl, V, Co, Cu, As, Nb, Ag, Sn, Sb, I, and Ta targets. *At. Data Nucl. Data Tables* **1972**, *4*, 129–207. [CrossRef]

57. Kwan, C.K.; Hsieh, Y.F.; Kauppila, W.E.; Smith, S.J.; Stein, T.S.; Uddin, M.N.; Dababneh, M.S. $e^{\pm}$-CO and $e^{\pm}$-CO_2 total cross-section measurements. *Phys. Rev. A* **1983**, *27*, 1328. [CrossRef]

58. Szmytkowski, C.; Zecca, A.; Karwasz, G.; Oss, S.; Maciag, K.; Marinkovic, B.; Brusa, R.S.; Grisenti, R. Absolute total cross sections for electron-CO_2 scattering at energies form 0.5 to 3000 eV. *J. Phys. B At. Mol. Phys.* **1987**, *20*, 5817. [CrossRef]

59. Nogueira, J.C.; Iga, I.; Chaguri, J.E. Total cross section measurements of electrons scattered by nitrogen and carbon dioxide in the energy range 500–3000 eV. *Rev. Bras. Fis.* **1985**, *15*, 224–234.

60. Garcia, G.; Manero, F. Total cross sections for electron scattering by CO_2 molecules in the energy range 400–5000 eV. *Phys. Rev. A* **1996**, *53*, 250. [CrossRef] [PubMed]

61. Hoffman, K.R.; Dababneh, M.S.; Hsieh, Y.F.; Kauppila, W.E.; Pol, V.; Smart, J.H.; Stein, T.S. Total-cross-section measurements for positrons and electrons colliding with H_2, N_2, and CO_2. *Phys. Rev. A* **1982**, *25*, 1393. [CrossRef]

62. Shilin, X.; Fang, Z.; Liqiang, Y.; Changqing, Y.; Kezun, X. Absolute total cross section measurement for electron scattering on in the energy range 600–4250 eV. *J. Phys. B At. Mol. Opt. Phys.* **1997**, *30*, 2867. [CrossRef]

63. Jain, A.; Baluja, K.L. Total (elastic plus inelastic) cross sections for electron scattering from diatomic and polyatomic molecules at 10–5000 eV: H_2, Li_2, HF, CH_4, N_2, CO, C_2H_2, HCN, O_2, HCl, H_2S, PH_3, SiH_4, and CO_2. *Phys. Rev. A* **1992**, *45*, 202. [CrossRef]

64. Hwang, W.; Kim, Y.K.; Rudd, M.E. New model for electron-impact ionization cross sections of molecules. *J. Chem. Phys.* **1996**, *104*, 2956–2966. [CrossRef]

65. Asundi, R.K.; Craggs, J.D.; Kurepa, M.V. Electron attachment and ionization in oxygen, carbon monoxide and carbon dioxide. *Proc. Phys. Soc. (1958–1967)* **1963**, *82*, 967. [CrossRef]

66. Craggs, J.D.; Tozer, B.A. The attachment of slow electrons in carbon dioxide. *Proc. R. Soc. Lond. Ser. A Math. Phys. Sci.* **1960**, *254*, 229–241.

67. Rapp, D.; Englander-Golden, P. Total cross sections for ionization and attachment in gases by electron impact. I. Positive ionization. *J. Chem. Phys.* **1965**, *43*, 1464–1479. [CrossRef]

68. Orient, O.J.; Strivastava, S.K. Electron impact ionisation of H_2O, CO, CO_2 and CH_4. *J. Phys.B At. Mol. Phys.* **1987**, *20*, 3923. [CrossRef]

69. Freund, R.S.; Wetzel, R.C.; Shul, R.J. Measurements of electron-impact-ionization cross sections of N_2, CO, CO_2, CS, S_2, CS_2, and metastable N_2. *Phys. Rev. A* **1990**, *41*, 5861. [CrossRef] [PubMed]

70. Straub, H.C.; Lindsay, B.G.; Smith, K.A.; Stebbings, R.F. Absolute partial cross sections for electron-impact ionization of CO_2 from threshold to 1000 eV. *J. Chem. Phys.* **1996**, *105*, 4015–4022. [CrossRef]

71. Mayol, R.; Salvat, F. Total and transport cross sections for elastic scattering of electrons by atoms. *At. Data Nucl. Data Tables* **1997**, *65*, 55–154. [CrossRef]

72. Kimura, M.; Sueoka, O.; Hamada, A.; Takekawa, M.; Itikawa, Y.; Tanaka, H.; Boesten, L. Remarks on total and elastic cross sections for electron and positron scattering from CO_2. *J. Chem. Phys.* **1997**, *107*, 6616–6620. [CrossRef]

73. Nakamura, Y. Drift Velocity and Longitudinal Diffusion Coefficient of Electrons in CO_2? Ar Mixtures and Electron Collision Cross Sections for CO_2 Molecules. *Aust. J. Phys.* **1995**, *48*, 357–364. [CrossRef]

74. Charlton, M.; Griffith, T.C.; Heyl, G.R.; Wright, G.L. Total scattering cross sections for low-energy positrons in the molecular gases H_2, N_2, CO_2, O_2 and CH_4. *J. Phys. B At. Mol. Phys.* **1983**, *16*, 323. [CrossRef]

75. Charlton, M.; Griffith, T.C.; Heyl, G.R.; Wright, G.L. Total scattering cross sections for intermediate-energy positrons in the molecular gases H_2, O_2, N_2, CO_2 and CH_4. *J. Phys. B At. Mol. Phys.* **1980**, *13*, L353. [CrossRef]

76. Zecca, A.; Perazzolli, C.; Moser, N.; Sanyal, D.; Chakrabarti, M.; Brunger, M.J. Positron scattering from carbon dioxide. *Phys. Rev. A* **2006**, *74*, 012707. [CrossRef]

77. Singh, S.; Antony, B. Study of inelastic channels by positron impact on simple molecules. *J. Appl. Phys.* **2017**, *121*, 244903. [CrossRef]